HHS Public Access

Author manuscript

Cell Rep. Author manuscript; available in PMC 2023 December 19.

Published in final edited form as:

Cell Rep. 2023 November 28; 42(11): 113449. doi:10.1016/j.celrep.2023.113449.

Keratinocyte FABP5-VCP complex mediates recruitment of neutrophils in psoriasis

Jiaqing Hao[1,7], **Jianyu Yu**[1,7], **Matthew S. Yorek**[1], **Chi-Li Yu**[2], **R. Marshall Pope**[2], **Michael S. Chimenti**[3], **Yiqin Xiong**[1], **Aloysius Klingelhutz**[4], **Ali Jabbari**[5,6], **Bing Li**[1,8,*]

[1]Department of Pathology, University of Iowa, Iowa City, IA, USA

[2]Proteomics Facility, University of Iowa, Iowa City, IA, USA

[3]Iowa Institute of Human Genetics, University of Iowa, Iowa City, IA, USA

[4]Department of Microbiology and Immunology, University of Iowa, Iowa City, IA, USA

[5]Department of Dermatology, University of Iowa, Iowa City, IA, USA

[6]Iowa City VA Medical Center, Iowa City, IA, USA

[7]These authors contributed equally

[8]Lead contact

SUMMARY

One of the hallmarks of intractable psoriasis is neutrophil infiltration in skin lesions. However, detailed molecular mechanisms of neutrophil chemotaxis and activation remain unclear. Here, we demonstrate a significant upregulation of epidermal fatty acid binding protein (E-FABP, FABP5) in the skin of human psoriasis and psoriatic mouse models. Genetic deletion of FABP5 in mice by global knockout and keratinocyte conditional (Krt6a-Cre) knockout, but not myeloid cell conditional (LysM-Cre) knockout, attenuates psoriatic symptoms. Immunophenotypic analysis shows that FABP5 deficiency specifically reduces skin recruitment of $Ly6G^+$ neutrophils. Mechanistically, activated keratinocytes produce chemokines and cytokines that trigger neutrophil chemotaxis and activation in an FABP5-dependent manner. Proteomic analysis further identifies that FABP5 interacts with valosin-containing protein (VCP), a key player in NF-κB signaling activation. Silencing of FABP5, VCP, or both inhibits NF-κB/neutrophil chemotaxis signaling. Collectively, these data demonstrate dysregulated FABP5 as a molecular mechanism promoting NF-κB signaling and neutrophil infiltration in psoriasis pathogenesis.

*Correspondence: bing-li@uiowa.edu.

AUTHOR CONTRIBUTIONS

J. H., J.Y., M.S.Y., and C.-L.Y. performed experiments and analyzed the data. C.-L.Y. and R.M.P. did mass spectrum analysis. Y.X. helped with reading the histological slides. M.S.C. did the pathway analysis. A.K. provided the human keratinocyte cell line and helped with paper writing. A.J. provided human samples and helped with paper writing. B.L. designed experiments and wrote the paper.

DECLARATION OF INTERESTS

The authors declare no competing interests.

SUPPLEMENTAL INFORMATION

Supplemental information can be found online at https://doi.org/10.1016/j.celrep.2023.113449.

In brief

Hao et al. show that FABP5 expression in keratinocytes promotes psoriasis pathogenesis through enhancing neutrophil infiltration and activation. FABP5 represents a promising therapeutic target for the treatment of psoriasis.

Graphical Abstract

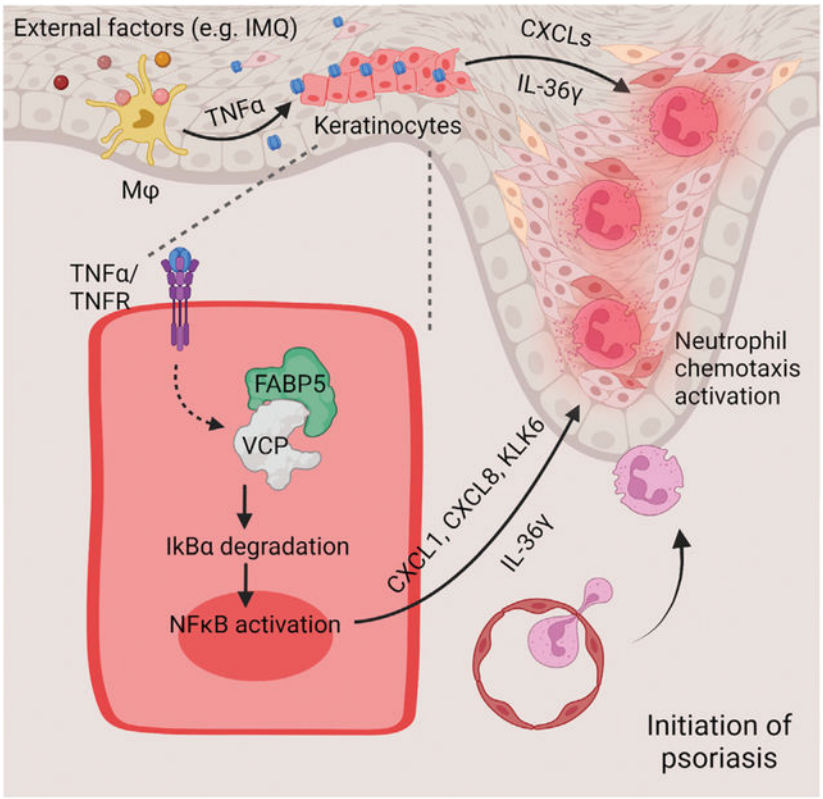

INTRODUCTION

Characterized with erythema, induration, desquamation, and plaques, psoriasis was historically considered as a keratinocyte-mediated skin disease.[1] To determine the mechanisms of psoriasis pathogenesis, multiple psoriatic animal models have been established, among which imiquimod (IMQ)-induced psoriasis model is widely used to mimic human psoriasis development.[2] Evidence from clinical and animal studies suggests that multiple types of skin resident cells, including keratinocytes and different immune cells, are involved in psoriasis pathogenesis.[3] However, the underlying molecular and cellular mechanisms of how different types of skin cells interact with each other in psoriasis initiation and development remain unclear.

Currently, most biological therapies for psoriasis are focused on inhibiting the proinflammatory function of immune cells by blocking the IL-23/IL-17/IL-22 axis.[4–7] Although attenuating the psoriatic symptoms, these treatments showed little evidence of full recovery of patients from psoriasis, suggesting that other types of inflammatory cells are

involved in psoriasis pathogenesis. Interestingly, as the first line of defense in the innate arm of immune responses, neutrophils have been shown to accumulate in the skin of psoriasis patients and function as a hallmark of psoriatic inflammation.[8,9] Psoriasis, especially pustular psoriasis, is characterized by excessive neutrophil infiltration, and neutrophil depletion has been shown to significantly improve the treatment of pustular psoriasis.[10] Despite the evidence that neutrophils are involved in psoriasis pathogenesis, it remains largely unknown how neutrophils are recruited and activated for psoriasis development.

The family of fatty acid binding proteins (FABPs) consists of at least nine members of 14–15 kDa proteins, facilitating fatty acid transportation and responses inside cells.[11] Recent studies indicate their pivotal roles in mediating obesity-associated diseases, including diabetes, cardiovascular diseases, cancer, and COVID-19.[12–16] Individual FABPs were termed according to the tissue where they were first identified, such as adipose FABP (A-FABP or FABP4) and epidermal FABP (E-FABP, or FABP5). Cloned from epidermis tissues in 1993, FABP5 has been shown to regulate proliferation and differentiation of human keratinocytes in both normal and psoriatic epidermis.[17,18] Hydrophobic ligands transported by FABP5 can augment the transcriptional activity of peroxisome proliferator-activated receptors (PPAR) β/δ to promote cell proliferation in different disease settings.[19] Our previous studies demonstrate that FABP5 is critical in mediating depilatory-induced acute skin inflammation and in high fat diet-induced chronic skin lesions.[20–24] Thus, we hypothesized that FABP5 might play a previously unappreciated role in psoriasis pathogenesis.

Here, we demonstrated that FABP5 was specifically upregulated in psoriatic skin tissue compared with healthy skin tissue. After showing an indispensable role of FABP5 using FABP5 whole-body knockout mice, we further identified that FABP5 expression in keratinocytes, but not in macrophages, contributed to IMQ-induced psoriatic-like inflammation using FABP5 conditional knockout mouse models. Importantly, we demonstrated a molecular mechanism by which FABP5 promoted TNF-α-induced NF-κB signaling by forming a complex with valosin-containing protein (VCP) in keratinocytes. The FABP5/VCP/NF-κB signaling axis enhanced the production of chemokines and cytokines (e.g., CXCLs and IL-36γ) for subsequent neutrophil chemotaxis and activation. These data provided evidence that FABP5 mediates inflammatory signaling in keratinocytes, coordinating neutrophil infiltration and activation, thus playing a critical role in psoriasis initiation and pathogenesis.

RESULTS

Psoriasis is associated with elevated levels of FABP5 expression

The development of psoriasis is associated with dysregulated lipid metabolism and metabolic syndrome.[25,26] We and others have shown that FABPs, especially FABP5, play a pivotal role in regulating metabolic and inflammatory pathways in keratinocytes and immune cells.[15,20,21,27] Despite first being cloned from psoriatic skin, the role of FABP5 in psoriasis pathogenesis remains largely unknown. Here, we analyzed expression levels of FABP family members (FABP1 to FABP7) in the skin of healthy individuals and psoriatic patients using publicly accessible databases from Gene Expression Omnibus. In

the GSE14905 dataset consisting of 21 healthy individuals and 33 psoriasis patients, FABP5, a predominant FABP member in the skin, was significantly upregulated in the psoriatic skin (Figures 1A and S1A–S1F). Consistent with these observations, the GSE13355 dataset, which included 64 healthy individuals and 58 psoriasis patients showed the same trend of elevated FABP5 expression in psoriasis patients (Figures 1B and S1G–S1L). To confirm the gene expression results in the datasets, we collected normal and psoriatic skin tissues and measured FABP5 expression at the protein level. FABP5 was predominantly expressed in the epidermis in both normal and psoriatic skin. Similar to the gene expression data, FABP5 was remarkably upregulated in the differentiated keratinocytes across the epidermal layer in psoriatic skin compared with normal skin (Figure 1C). Recapitulating features of psoriasis with the IMQ-induced mouse models, we observed that IMQ treatment significantly upregulated FABP5 expression in the epidermis at both mRNA levels (Figure 1D) and protein levels (Figure 1E). Altogether, these data demonstrated that psoriasis development was associated with elevated expression of FABP5, suggesting an underappreciated role of FABP5 in psoriasis pathogenesis.

FABP5 deficiency in mice attenuates psoriatic symptoms and neutrophil recruitment

To investigate the role of FABP5 in psoriasis development, we used Fabp5 global knockout ($Fabp5^{-/-}$) mice and their wild-type (WT) littermates and evaluated their psoriatic features, including erythema, desquamation, and induration, in response to IMQ treatment. Compared with IMQ-treated WT mice, $Fabp5^{-/-}$ mice exhibited significantly reduced skin inflammation on back skin as quantified by individual and cumulative scores of psoriatic features (Figures 2A and 2B). We also measured the thickness of IMQ-treated ears in these mice. FABP5 deficiency significantly attenuated skin thickness as shown in Figures 2C and 2D. Of note, inflammatory cell infiltration in the ears of $Fabp5^{-/-}$ mice was apparently reduced when compared with WT mice (Figure 2E). To further determine the inflammatory immune cell profiles in the skin of WT and $Fabp5^{-/-}$ mice, we collected tissues, including dermis and epidermis, ear, spleen, peripheral blood, and bone marrow, from these mice and analyzed their immunophenotypes in response to IMQ treatment. Interestingly, when compared with $Fabp5^{-/-}$ mice, WT mice were associated with a significant increase of neutrophils ($Ly6G^{+}$) in the ear (Figure 2F), dermis (Figure 2G), peripheral blood (Figure 2H), and epidermis (Figure S2A), but not in bone marrow (Figure S2B) and spleen (Figure S2C). In contrast, except $CD8^{+}$ T cells that were trended higher in the WT skin, there were no differences of other major immune cell populations, including macrophages ($CD11b^{+}F4/80^{+}$), $CD4^{+}$ and γδT cells between WT and $Fabp5^{-/-}$ mice (Figures S2D–S2H). Given that neutrophils mediated early responses to inflammatory stimuli,[28] the increase of neutrophil infiltration in WT mice suggested that elevated FABP5 expression in skin functioned to induce neutrophil recruitment during the onset of psoriatic inflammation.

FABP5 expression in keratinocytes contributes to neutrophil-initiated psoriatic inflammation

FABP5 was expressed in both keratinocytes and macrophages in the skin.[20] To determine the cell-specific role of FABP5 in psoriasis development, we developed Fabp5 floxed mice ($Fabp5^{f/f}$) by flanking exons 2 and 3 of the Fabp5 gene with *LoxP* sites (Figure S3A). $Fabp5^{f/f}$ mice were then crossed with Krt6A-Cre and LysM-Cre mice to

generate keratinocyte or macrophage conditional knockout mice, respectively (Figure S3B). Conditional knockout and control mice were identified using direct PCR genotyping for flox recombination and the Cre transgenes (Figures S3C and S3E). To validate the efficiency of Fabp5-specific deletion, keratinocytes and peritoneal macrophages were collected and analyzed for FABP5 expression using intracellular flow staining. Indeed, Fabp5$^{f/f}$ Krt6A-Cre mice exhibited specific deletion of Fabp5 in keratinocytes (Figures S3F–S3I), whereas Fabp5$^{f/f}$ LysM-Cre mice exhibited specific deletion of Fabp5 in macrophages (Figures S3J–S3M).

Next, we evaluated the cell-specific role of FABP5 in psoriasis development and neutrophil infiltration using these conditional knockout mice. In response to IMQ treatment, Fabp5$^{f/f}$ Krt6A-Cre^{+} mice showed alleviated psoriasis symptoms demonstrated by reduced desquamation and acanthosis when compared with the Fabp5$^{f/f}$ Krt6A-Cre^{-} littermates (Figure 3A). The quantitative cumulative scores, including erythema, desquamation, and acanthosis, were significantly reduced in Fabp5$^{f/f}$ Krt6A-Cre^{+} mice (Figure 3B). The ear thickness of Fabp5$^{f/f}$ Krt6A-Cre^{+} mice was also significantly less than WT controls (Figure 3C). We further analyzed the immunophenotype from different tissues of these mice. Similar to the Fapb5 global knockout, specific deletion of Fabp5 in keratinocytes reduced the infiltration of neutrophils in the ear, dermis, and peripheral blood (Figures 3D–3F), but there were no significant differences for macrophages and T cells in these mice (Figures S4A–S4D). These data suggested that specific deletion of Fabp5 in keratinocytes attenuated IMQ-induced psoriasis-like skin inflammation and neutrophil infiltration. We further evaluated the role of FABP5 expression in macrophages in psoriasis development using the Fabp5$^{f/f}$ LysM-Cre^{+} and Fabp5$^{f/f}$ LysM-Cre^{-} mice. IMQ treatment induced similar psoriasis symptoms in these mice (Figure 3G), but there were no differences regarding the cumulative scores (Figure 3H), ear thickness (Figure 3I), and neutrophil infiltration in the ear, dermis, and PBMC (Figures 3J–3L) between Fabp5$^{f/f}$ LysM-Cre^{+} and Fabp5$^{f/f}$ LysM-Cre^{-} mice, suggesting a dispensable role of FABP5 in macrophages in the development of IMQ-induced psoriasis. Altogether, data from these mouse models demonstrated that the function of Fabp5 in keratinocytes, but not in myeloid-derived macrophages, is pivotal for neutrophil-mediated psoriatic inflammation.

Human psoriasis is associated with neutrophil-related signaling pathways

To understand signaling pathways underlying FABP5-enhanced neutrophil infiltration in psoriatic inflammation, we further analyzed the GSE14905 microarray dataset. Based on the profile of the Uniform Manifold Approximation and Projection, healthy individuals and psoriasis patients fell into two entirely different clusters (Figure 4A), suggesting a distinct gene expression pattern in psoriasis. Differentially expressed genes (DEGs) with an adjusted p value <0.05 between these two groups were shown in the volcano plot with genes related to psoriatic inflammation and neutrophil chemotaxis and activation, such as CXCL8, CXCL9, IL-36γ, KLK6, etc. (Figure 4B). Gene pathway analysis of the DEGs showed that chemokine- and cytokine-mediated signaling pathways were significantly different between the two groups (Figures S5A and S5B). More specifically, genes regulating neutrophil recruitment (e.g., CXCL1, CXCL8) and activation (e.g., IL-36γ) were significantly upregulated in the psoriasis group (Figures 4C–4E and S5C). Gene ontology

term analysis confirmed that neutrophil chemotaxis and migration were among the top biological process terms enriched in psoriasis (Figure 4F). Of note, TRRUST database analysis showed NF-κB signaling, including RELA, NF-κB1, IKBKB, etc., as the main upstream transcription factors in regulating chemokine and cytokine signaling pathways associated with neutrophil recruitment and activation in psoriasis (Figure 4G). Using the IMQ-induced psoriasis mouse model, we further confirmed that genes related to neutrophil recruitment and activation, including CXCL1, CXCL2, IL-36γ, and TNF-α (Figure 4H), were upregulated in response to IMQ treatment. Interestingly, genes related to T cell activation, such as IFN-γ, IL-23, IL-17, and IL-12 were barely detectable in the early stage of the disease, suggesting a critical role of neutrophils, but not T cells, in the initiation of psoriasis.

FABP5 mediates chemokine signals in keratinocytes for neutrophil chemotaxis

To test if FABP5 is crucial in mediating neutrophil-related chemokine/cytokine signals in psoriasis, we first measured their expression levels in the skin of WT and Fabp5$^{-/-}$ mice treated with IMQ. As expected, Fabp5 deficiency significantly reduced CXCL1, CXCL2, and IL-36γ expression (Figures 5A–5D) but did not affect IL-17 production in skin T cells (Figures S6A–S6C). To further verify the critical role of FABP5 in human keratinocytes, we knocked down FABP5 expression in human HaCaT cells using siRNA and measured the levels of genes related to neutrophil chemotaxis and activation (Figure 5E). Unlike skin macrophages/DCs, keratinocytes did not express TLR7.[29] As such, IMQ treatment did not directly induce upregulation of CXCL1, CXCL2, CXLC8, IL-36γ, and KLK6 in HaCaT cells. In contrast, treatment of HaCaT cells with TNF-α significantly upregulated the production of these chemokines/cytokines in an FABP5-dependent manner (Figures 5F–5J). FABP5 knockdown did not affect other psoriasis-related inflammatory factors, including CXCL9, KLK8, and TNF-α (Figures S6D–S6F), suggesting a specific role of FABP5 in promoting neutrophil chemotaxis in psoriasis. Of note, TNF-α was mainly produced by epidermal Langerhans cells and dermal macrophages/DCs.[30,31] FABP5 deficiency had no impact on IMQ-induced TNF-α production in bone marrow-derived macrophages and DCs (Figures S6G and S6H) and in skin macrophages (Figure S6I). These data suggested that FABP5 did not influence TNF-α production in immune cells but was involved in the TNF-α-induced neutrophil chemokine signaling in keratinocytes. To further confirm the FABP5/neutrophil connection, we observed that high expression of FABP5 in human psoriatic keratinocytes was associated with increased infiltration of neutrophils (Figure 5K). Altogether, these data demonstrated a role of FABP5 in promoting neutrophil chemotaxis signaling in keratinocytes.

FABP5 binds VCP for the activation of the TNF-α/NF-κB signaling

Given that NF-κB is the main transcriptional factor for TNF-α-induced chemokine signaling,[32,33] we further determined the molecular mechanism by which FABP5 mediated TNF-α/NF-κB signaling in keratinocytes. Proteomic analysis was used to screen possible endogenous FABP5-binding partners (Figure 6A). Lysates of TNF-α-treated HaCaT cells were used for immunoprecipitation (IP) assays with specific anti-FABP5 or a control antibody, which led us to identify several FABP5-binding partners that were pulled down by the anti-FABP5 antibody (Figures 6B and 6C). Among these bands, VCP was the top

hit in the proteomic analysis due to its abundance and specificity in the samples pulled down by the anti-FABP5 antibody (Figure S7A). The interaction of FABP5/VCP was further confirmed in HaCaT cells using coIP assays pulling down either with anti-FABP5 (Figure 6D) or with anti-VCP (Figure 6E). These two-way coIP assays demonstrated that FABP5 and VCP interacted in a natural state. Consistent with the IP and proteomics analyses, confocal staining validated the colocalization of FABP5 and VCP in HaCaT cells (Figures 6F, 6G, and S7B).

VCP is known to play an essential role in mediating the proteolysis of IκBα, an inhibitor of NF-κB, thus the VCP complex is critical for NF-κB activation.[34,35] Given the findings of FABP5/VCP interactions in keratinocytes, we speculated that FABP5 was a crucial partner for VCP-mediated IκBα/NF-κB signaling activation. To determine the role of FABP5 in the activation of IκBα, we first silenced the endogenous FABP5 in the HaCaT cells using RNAi (Figures 6H and 6I), and then measured protein levels of VCP and phospho-IκBα, and phospho-NFκB in the silenced vs. control cells in response to TNF-α treatment (Figure 6H). While there were no significant differences in the levels of VCP (Figure S7C) between FABP5-silenced or control cells, phosphorylated IκBα (S32) and phosphorylated NF-κB p65 (S536) were significantly lower in the FABP5-silenced cells (Figures 6J and 6K), suggesting a critical role of FABP5 in proteolysis of IκBα, thus leading to NF-κB phosphorylation and activation in keratinocytes. To further confirm the FABP5/VCP complex in regulating NF-κB signaling, we silenced the expression of FABP5, VCP, or both in keratinocytes and compared with the downstream chemokine/cytokine production. Compared with non-targeting siRNA control (siNC), silencing FABP5 (siFABP5) did not affect VCP expression and silencing VCP (siVCP) did not affect FABP5 expression either (Figures S7D and S7E), suggesting that FABP5 and VCP did not regulate each other, although they bound together as a complex. Silencing either FABP5 or VCP significantly reduced the expression of CXCL2, CXCL8, IL-36γ, and KLK6, but not KLK8 and TNF-α, in keratinocytes. Interestingly, dual silence of FABP5 and VCP exhibited similar inhibition of these factors as single silencing of either one (Figures S7F–S7K). These data suggested that FABP5 interacted with VCP as a complex in activating NF-κB/neutrophil chemokine signaling in keratinocytes.

DISCUSSION

Observed in unearthed Egyptian mummies, psoriasis has existed since ancient times, and remains the most prevalent chronic inflammatory skin disease. Although current treatments, including phototherapy, topical and systemic therapies (e.g., corticosteroids, cyclosporin), and biological therapy (e.g., antibodies targeting specific cytokines), could help to relieve psoriatic symptoms, there is still no cure for psoriasis. The duration and prevalence of psoriasis indicate an incomplete understanding of the cellular and molecular mechanisms involved in its pathogenesis.[36–39] Using psoriatic human specimens and genetically modified mouse models, we identified a crucial role of FABP5 in psoriasis development. Specifically, our studies demonstrate that FABP5 is upregulated in the epidermis of psoriatic skin, leading to enhanced inflammatory TNF-α/NF-κB signaling in keratinocytes, followed by neutrophil chemotaxis and activation. Genetic deletion of FABP5 in global or keratinocyte-specific knockout mice significantly reduced the production of chemokines

(e.g., CXCLs, IL-36γ) for neutrophil recruitment and attenuated psoriatic inflammation and symptoms. Therefore, FABP5 represents a host-derived molecular mechanism underlying psoriasis development.

Recent studies suggest that crosstalk between keratinocytes and infiltrated immune cells contributes to psoriasis pathogenesis.[40] However, the exact molecular mechanisms initiating the crosstalk between keratinocytes and immune cells remain unknown. Given that severe psoriasis patients are usually associated with metabolic syndrome, we analyzed public psoriasis databases and human psoriatic skin tissues by focusing on metabolism-related signaling and found that FABP5, a skin lipid chaperone, was significantly upregulated in psoriatic skin samples. Importantly, deletion of FABP5 in mice prevented IMQ-induced psoriatic inflammation and symptoms without affecting IL-17 signaling in T cells. To further determine the mechanisms of action of FABP5, we established FABP5 conditional knockout mice, and confirmed that FABP5 expression in keratinocytes, but not in macrophages, contributed to psoriasis development. Moreover, elevated FABP5 was associated with increased infiltration of neutrophils during psoriasis development in these mouse models. These data suggest FABP5 as an underlying molecular link mediating the crosstalk between keratinocytes and neutrophils for the development of psoriasis.

As the most abundant innate immune cell, the presence of neutrophils is considered a histopathologic hallmark of psoriatic skin lesions.[41] Through reactive oxygen species, degranulation, and extracellular trap formation, neutrophils bridge innate and adaptive immunity and contribute to psoriasis initiation and progression.[42,43] Attempts to reduce neutrophil infiltration and activation has become an interest for psoriasis management.[44] In dissecting how FABP5 promotes neutrophil recruitment, we identified that FABP5 deficiency significantly impairs the production of chemokines for neutrophil chemotaxis, including CXCL1, CXCL2 in murine models, and CXCL1, CXCL2, and CXCL8 in human keratinocytes. Moreover, IL-36γ, a well-known neutrophilic inflammatory cytokine,[45,46] was also downregulated in the absence of FABP5. In line with our previous findings that FABP5 regulates IL-36γ production and neutrophil recruitment in other skin models,[21,22] FABP5 is likely to be a critical regulator in mediating neutrophilic inflammation.

As an intracellular lipid chaperone, FABP5 is known to bind certain hydrophobic ligands for nuclear translocation and activation of PPARβ/δ.[47] The FABP5/PPARβ/δ axis has been shown to promote cell proliferation of several epithelial-derived tumors.[19,48] Moreover, FABP5 deficiency is associated with reduced differentiation and NF-κB activity in keratinocytes,[27] but the how FABP5 regulates NF-κB signaling remains unknown. In this study, we performed proteomic analysis using proteins immunoprecipitated with anti-FABP5 antibody in TNF-α-treated human keratinocytes, and found that FABP5 co-precipitated with VCP, an essential ATPase for IκBα degradation and NFκB activation.[49,50] The finding of the FABP5/VCP complex in regulating NF-κB signaling was demonstrated by several observations: (1) mass spectrometry analysis showed specific binding of VCP with proteins pulled down by the anti-FABP5 antibody, (2) two-way coIP assays with either anti-FABP5 or anti-VCP antibodies confirmed the FABP5/VCP complex in keratinocytes, (3) confocal analysis showed the co-localization of FABP5/VCP in keratinocytes, (4) silencing FABP5 reduced phosphorylated IκBα and activation of NF-κB signaling in human keratinocytes,

and (5) dual silencing of FABP5 and VCP exhibited a similar effect as single silencing either of them on neutrophil chemokine production. Given the mounting evidence of the individual roles of FABP5, VCP, and NF-κB in the pathogenesis of psoriasis,[27,51,52] our findings of the FABP5/VCP complex in regulating NF-κB signaling converged these observations together, thus uncovering a mechanisms by which FABP5 integrates inflammatory signaling and enhances crosstalk between keratinocytes and neutrophils for the initiation of psoriasis.

It is worth noting that, in IMQ-induced psoriasis models, skin macrophages/DCs, but not keratinocytes, highly express TLR7, which responds to IMQ treatment by production of inflammatory cytokines (e.g., TNF-α).[53,54] FABP5 conditional knockout in macrophages in the LysM-Cre mice did not protect against IMQ-induced psoriatic inflammation, suggesting a dispensable role of FABP5 in macrophages in the TLR7-initiated signals. Indeed, we did not observe any significant differences in the production of cytokines (e.g., TNF-α, IL-23, IL-17) in LysM-Cre WT and knockout mice. Interestingly, FABP5 conditional knockout in keratinocytes in the Krt6A-Cre mice significantly protected mice from IMQ-induced neutrophil infiltration and psoriatic inflammation. In line with the role of regulating keratinocyte/neutrophil interaction, FABP5 has also been shown to promote keratinocyte differentiation.[27] All these lines of evidence suggest that dysregulated increase of FABP5 expression in keratinocytes plays a critical role in the onset and development of psoriatic symptoms. While multiple immune cell subsets (e.g., macrophage, T cells, DCs) and inflammatory mediators (e.g., IL-17, IL-23, IL-36, TNF-α) have been shown to be important in IMQ mouse models, the current studies identifying FABP5 as an underlying molecular sensor linking inflammatory cascades to neutrophil infiltration offer a mechanism and therapeutic target for psoriatic onset and treatment.

Limitations of the study

With the IMQ-induced acute model of human psoriasis, FABP5 has been identified as a primary mediator of neutrophil chemotaxis. However, considering the chronic nature of human psoriasis, FABP5 might also play roles in other inflammatory pathways, such as dysregulated keratinocyte proliferation, and cytokine productions in skin γδ T cells, etc. In addition, epidemiological research shows that obesity elevates the risk of psoriasis and intensifies psoriatic inflammation. However, the molecular mechanisms underlying the obesity/psoriasis associations remain largely undefined. It is possible that FABP5 may integrate the metabolic and inflammatory pathways triggered by excessive fatty acids in obesity, thereby influencing the pathogenesis of obesity-associated psoriasis.

STAR★METHODS

RESOURCE AVAILABILITY

Lead contact—Further information and requests for reagents may be directed to and will be fulfilled by the Lead Contact, Bing Li (bing-li@uiowa.edu).

Materials availability—All unique/stable reagents generated in this study are available from the lead contact with a completed materials transfer agreement.

Data and code availability—All data generated in this study will be made available upon request from the lead contact. This paper does not report original code. Any additional information required to reanalyze the data reported in this paper is available from the lead contact upon request.

EXPERIMENTAL MODEL AND STUDY PARTICIPANT DETAILS

Mice and psoriasis-like skin mouse models—A series of C57BL/6 background mice, including Krt6A-Cre, LysM-Cre mice were purchased from Jackson Laboratory. Fabp5$^{f/f}$ mice and Fabp5$^{-/-}$ mice and their wild-type controls were maintained and bred under specific pathogen free conditions with water and regular chow *ad libitum* in the animal facility of the University of Iowa in accordance with the University of Iowa Institutional Animal Care and Use Committee.

Male mice at 8–12 weeks age were removed with commercially depilatory agents, facial hair removal cream (Nair, 400mg per mice), and monitored for another two days. The hair removed mice were then randomly treated with 15 mg IMQ cream (Perrigo, containing 5% IMQ) and placebo cream daily for seven consecutive days. Mice ear was directly treated with 5 mg IMQ cream and monitored the thickness daily. Considering the severe symptom on mouse models that are as similar as human PASI, we took severity scoring on erythema, induration, and desquamation. The cumulative score was calculated from these three parameters other than area because we artificially created a psoriasis mouse model on dorsal skin. The score is classified as five levels from 0 to 4, which 0 is the lowest indicating no severity and 4 is the highest severity. At the treatment endpoint (day seven), mice were sacrificed to analyze immunophenotype in different tissues.

Patient specimens—Formalin-fixed, paraffin-embedded tissue blocks from the University of Iowa Dermatopathology specimen archive were selected by interrogation of the archive records for the keyword of “psoriasis” in the diagnosis. Skin sections were cut and transported to the study team without further patient identifiers. The University of Iowa Institutional Review Board reviewed the study protocol (#202105091) prior to sample acquisition and classified the study as not human subjects research.

METHOD DETAILS

Psoriasis microarray gene expression and pathway analyses—Psoriasis-related gene expression datasets, GSE14905[55] and GSE13355,[56] were downloaded from Gene Expression Omnibus (GEO) database. GSE14905 dataset consists of extracted RNA from skin biopsies of 12 healthy donors and 33 psoriasis patients. Similarly, GSE13355 dataset contains RNA from skin biopsies of 64 healthy donors and 58 psoriasis patients. Relative expression of individual genes of psoriasis vs. healthy individuals was obtain from both datasets GSE14905 and GSE13355 and analyzed using GraphPad Prism 9 software. Adjusted p value and log2 fold change of differential gene expression (DEG) and clusters of psoriasis vs. healthy individuals in dataset GSE14905 was analyzed using on-site GEO2R tool, an R based tool. Upstream transcription factors in datasets were analyzed using the TRRUST, a reference database of human and mouse transcriptional regulatory interactions.[57] The DEGs from GEO dataset GSE14905 were analyzed using Advaita

Bio's iPathwayGuide[58,59] software to identify significantly impacted pathways, biological processes, molecular interactions, miRNAs, and upstream regulators.

Quantitative real-time PCR—RNA was extracted from skin tissues and HaCaT cells using PureLink RNeasy Mini Kit (Cat. #12183025, Invitrogen, Waltham, MA). The cDNA synthesis was performed with a QuantiTect Reverse Transcription Kit (Cat. #205314, Qiagen, Hilden, Germany) according to the manufacturer's instruction. Real-time PCR was performed with Power SYBR Green PCR Master Mix (Cat. #4368708, Applied biosystems, Waltham, MA) using StepOnePlus qPCR Systems (Applied Biosystems) to analyze the expression of target genes including FABP family, cytokines, chemokines using primers from IDT (see primer sequences in Table S1). Housekeeping genes for murine and human were Hprt1 and GAPDH, respectively.

Immunoprecipitation assay—HaCaT cells were cultured at 90% confluency in a 100-mm Petri dish and treated with recombinant human TNFα (Cat. #570104, Biolegend) for 5 min. Cells were washed with cold PBS twice, detached with scraper, and lysed with 500 μL IP lysis buffer (Cat. #87787, Thermo Scientific) containing 5 μL protease and phosphatase inhibitor cocktail (Cat. #PPC2020–1ML, Sigma) for 15 min at 4°C. After centrifugation at top speed for 10 min at 4°C, 50 μL of supernatant was collected as input and divided left into two parts. Endogenous FABP5 was pulled down with 1 μg anti-FABP5 polyclonal antibody (Cat.# PA5–80612, Fisher Scientific) using one part of the left supernatant with rotation at 4°C for overnight. The control rabbit IgG antibody (Cat. # ab37415, Abcam) was added to the remaining part of supernatant as an immunoprecipitation control. The Ag-Ab complex was added with 20 μL Protein G agarose beads (Cat#. 37478s, CST) and incubated 2 h with rotation at 4°C. The Ag-Ab-beads complex was centrifuged at 1000 rpm for 1 min at 4°C and washed for three times with cold PBS. The Ag-Ab-beads complex was added with SDS loading buffer containing 2-mercaptoethanol and boiled at 90°C for 5 min. Samples were used to perform Western blot or Mass spectrometry analysis.

PAGE and in-gel trypsin digestion—Forty-five microliters of IP enriched protein eluate were loaded on NuPage 4–12% Bis-Tris precast gels (Invitrogen, USA, Ref# NP0335BOX) and separated at 200V for 50min. 10 μL solution of mass ladder markers (Sharp pre-stained migration standards, Invitrogen) were loaded onto a separate gel lane to serve as a guide to molecular weight. The gel was stained using a mass spec compatible GelCode Blue Stain Reagent (ThermoScientific, USA, Ref# 24590) following the manufacturer's directions. A procedure slightly modified from the one described in[60] was used for in-gel digestion. Briefly, the targeted protein bands from PAGE gel were manually excised, cut into 1 mm^3 pieces, and washed in 100 mM ammonium bicarbonate: acetonitrile (1:1, v/v) and 25 mM ammonium bicarbonate/acetonitrile (1:1, v/v), respectively to achieve complete detaining. The gel pieces were further treated with ACN, to effectively "dry" the gel segments and then reduced in 50 μL of 20 mM DTT at 56°C for 60 min. After this, gel-trapped proteins were alkylated with 55 mM Chloroacetamide (CAM) for 30 min at room temperature in the dark. The gel pieces were washed with 25 mM ammonium bicarbonate: acetonitrile (1:1, v/v) twice to removed excess DTT and CAM and dehydrated in ACN. Then 50 μL of cold trypsin solution at 10 ng/μL in 25 mM ammonium bicarbonate

was added to the gel pieces and they were allowed to swell on ice for 60 min. Digestion was conducted at 37°C for 16 h. Peptide extraction was performed three times adding 100 μL of 65% acetonitrile/0.1% formic acid for 0.5 h; and combining the supernatants. The combined extracts were concentrated in a lyophilizer and rehydrated with 15 μL of Mobile Phase A.

LC-MS/MS—Mass spectrometry data were collected using a Q-Exactive Orbitrap mass spectrometer (Thermo Fisher Scientific, San Jose, CA) coupled to an Easy-nLC-1200 System (Proxeon P/N LC1400). Typically, the autosampler is set to aspirate 6 μL (estimated 0.4 μg) of reconstituted digest and load the solution on a 2 cm C18 trap (Thermo Scientific, Catalog. No. 164535) coupled to waste, HV and an analytical column through a microcross assembly (IDEX, P/N UH-752). Peptides are desalted on the trap using 16 μL mobile phase A in 4 min. The waste valve is then blocked, and a gradient begins flowing at 0.3 μL/min through a 50 cm Acclaim PepMap 100 C18 HPLC Columns (Thermo Scientific, Catalog. No. 164570).

Peptides were separated in-line with the mass spectrometer using an 88 min gradient composed of linear and static segments wherein buffer A is 0.1% formic acid and B is 90% ACN, 0.1% Formic acid. The gradient first holds at 4% for 3 min then makes the following transitions (%B, min): (2, 0), (3,3) (35, 63), (60, 73), (98, 78), (98, 88).

Tandem mass spectrometry on the Thermo Q-Exactive hf—Data acquisitions begin with a survey scan (m/z 375–1800) acquired on a Q-Exactive Orbitrap mass spectrometer (Thermo Fisher Scientific) at a resolution of 60,000 in the off axis Orbitrap segment (MS1) with Automatic Gain Control (AGC) set to 3E06 and a maximum injection time of 100 ms. MS1 scans are acquired every 3 s during the 88 min gradient described above. The most abundant precursors were selected among 2–6 charge state ions at a 1E05 AGC and 50 ms maximum injection time. Ions were isolated with a 1.6 Th window using the multi segment quadrupole and subject to dynamic exclusion for 30 s if they were targeted twice in the prior 30 s. Selected ions were then subjected to high energy collision-induced dissociation (HCD). Targeted precursors were fragmented by (HCD) at 30% collision energy in the HCD cell. HCD fragment ions were analyzed using the Orbitrap (AGC 1.2E05, maximum injection time 110 ms, and resolution set to 30,000 at 400 Th). MS2 data were recorded as centroid and the MS1 survey scans were recorded in profile mode.

Proteomics searches—Initial spectral searches were performed with both Proteome Discoverer 2.4 (ThermoFisher Scientific) and Byonic search engines (Protein Metrics ver. 2.8.2). Search databases were composed of the Uniprot KB for species 9606 (Human) downloaded 10/29/2022 containing 26586 sequences and Common contaminations. For Byonic searches, these two databases were directly concatenated. In either search an equal number of decoy entries were created and searched simultaneously by reversing the original entries in the target databases. Precursor and fragment mass tolerance was set to 10 ppm. A fixed 57 Da modification was assumed for cysteine residues while a variable Oxidation modification was allowed at methionine. A variable GG modification at lysine was set to monitor Ubiquitylation with potential phosphorylation accessed at Ser and Thr residues. Both Proteome Discoverer 2.4 and Byonic search results were combined and validated

using Scaffold ver. 5.0.2 (Proteome Software). Proteins assignments required a minimum of two peptides established at 1% FDR (Local FDR algorithm) and an overall 95% protein probability (assigned by Protein Prophet). Approximately 200 protein families (including common contaminants) were assigned at a total FDR to 1.2%.

Western blotting—Western blot was performed with samples from either HaCaT cell lysate or immunoprecipitation. Protein sample concentration was measured using the BCA assay kit (Cat. #23225, Thermo Scientific). The target protein involved in the NF-κB signaling pathway was detected using antibody sampler kit (Cat. #9936, CST). FABP5 and VCP levels were detected using anti-FABP5 polyclonal antibody (Cat.# PA5–80612, Invitrogen) and anti-human VCP monoclonal antibody (Cat# MA3–004, Invitrogen), separately. β-actin was used as a loading control. A BioRad system was used to capture images to determine the protein levels and ImageJ was used to perform relative protein quantification.

Flow cytometry analysis—Single suspension cells prepared from tissues of epidermis, dermis, PBMC, bone marrow, spleen, and ear. Surface staining in immune cells from these tissues were first blocked with anti-mouse CD16/32 (Cat. #101302, Biolegend) for 30 min at 4°C in PBS containing 1% FBS. Cells were washed and stained with following reagent in cold PBS: Zombie-violet (Cat. #423114, Biolegend) for live/dead cell staining, anti-mouse CD45-APC-Cy7 (Cat. #103116, Biolegend), CD11b-APC (Cat. #101212, Biolegend), anti-mouse TCR β/δ-BV510 antibody (Cat. #118131, Biolegend), anti-mouse CD4-BV510 (Cat. #100449, Biolegend), anti-mouse CD4-PE-Cy7 (Cat. #100422, Biolegend), anti-mouse CD8α-BV650 (Cat. #100741, Biolegend), anti-mouse Ly6G-PE (Cat. #127608, Biolegend), anti-mouse F4/80-AF488 (123120, Biolegend), anti-mouse NK1.1-PE/dazzle (Cat. #108748, Biolegend), anti-mouse CD3ε-BUV737 (612771, BD Bioscience), anti-mouse/human CD207 (Cat. #144204, Biolegend); For intracellular staining, cells were stained with surfaced antibodies as mentioned above for 30 min at 4°C in PBS. Cells were washed with PBS, fixed and permeabilized with Intracellular Staining Buffer Set (Cat. #00–5523-00, Invitrogen) according to the manufacturer's protocol. Cells were stained for 1 h at 4°C with different antibodies: anti-mouse/human cytokeratin 6A antibody (Cat. #10590–1-AP, Thermo Fisher), anti-mouse/human FABP5 (Cat. #AF1476, R&D Systems), secondary antibody for donkey anti-goat IgG-Alexa Fluor 647 (Cat. #705–606-147, Jackson ImmunoResearch), and secondary antibody for donkey anti-rabbit IgG-DyLight 488 (Cat. #406404, Biolegend). Skin macrophages were stimulated with Cell Activation Cocktail (Cat. #423303, Biolegend) for 6 h, and detected TNFα levels with intracellular staining using anti-mouse TNFα-APC-Cy7 (Cat. #506344, Biolegend). Cells were acquired either by BD FACS Fortessa or Cytek Aurora System. All the data were analyzed using FlowJo 10.1.

Skin tissue preparation—The isolation protocol of keratinocytes and dermis cells were followed from the previous studies (Morris et al., 2019; Zhang et al., 2019; Yin et al., 2021). Briefly, the mouse skin was removed using thumb forceps and scissors after seven consecutive days of treatment with IMQ cream or placebo cream. The removed skin was placed epidermis side down on the cover of a 100 mm Petri dish containing cold PBS, and the subcutaneous fat tissue was scraped off using a curved thumb forceps and the spine

of the surgical scalpel blade. The remaining skin tissue was sliced into about 0.5 × 1 cm strips and incubated with 20 mL of 0.25% trypsin-EDTA at 32°C for 1.5 h. The epidermis tissue and dermis tissue were separated with a scalpel blade in cold PBS. Keratinocytes were acquired from epidermis tissue by dispersing with a pipette for at least 10 min and being filtered through a 40 μM cell strainer. Dermis tissue and ear tissue were cut into small pieces and digested in the triple enzyme solution consisting of 0.2 mg/mL hyaluronidase (Sigma-Aldrich, St. Louis, MO), 0.02 mg/mL DNase I (Roche, Mannheim, Germany), and 0.5 mg/mL collagenase type II (Worthington Biochemical, Lakewood, NJ) in 5% fetal bovine serum RPMI-1640 medium for 45 min at 37°C. Dermis cells were acquired by filtering with a 40 μM cell strainer.

RNAi—Specific duplex small interfering RNA targeting human FABP5, VCP and its control were ordered from Integrated DNA Technologies. To silence FABP5, VCP or both, HaCaT cells were transfected with respective siRNAs (40 nM) using jetPRIME(Cat.# 101000046, Polyplus). The efficiency was confirmed using real-time PCR and Western blot.

Cell culture—HaCaT cells were cultured with DMEM medium containing 10% FBS and antibiotics (Cat. #30–2300, ATCC). HaCaT cells are a spontaneously immortalized human keratinocyte cell line.[61] To investigate the effect of FABP5 deficiency in NF-κB signaling activation, HaCaT cells were transfected with siRNA targeting human FABP5 and its control. After 48 h of culture, cells were treated with 20 ng/mL TNFα to activate NF-κB signaling for 0, 5, 15, 30, and 90 min. At the indicated time, cells were washed with cold PBS twice, and lysed with RIPA buffer containing 5 μL protease and phosphatase inhibitor cocktail for 15 min on ice. Supernatants were collected after centrifugation at top speed at 4°C. The concentration of cell protein was determined using BCA assay kit (Cat. #23225, Thermo Scientific).

For BMDM and BMDC culture *in vitro*, bone marrow cells FABP5 global knockout male mice and control wildtype mice were seeded in 100 mm Petri dish with 10 mL complete medium containing RPMI 1640, 5% FBS, and 10 μg/mL gentamicin at 37°C. Non-adherent cells were collected after 2 h, and seeded in a new Petri dish at the concentration of 4×10^6 in 15 mL complete medium supplemented with either 20 ng/mL GM-CSF for BMDC or 40 ng/mL M-CSF for BMDM. Half of the medium was removed on days 2 and 5, and replaced with fresh complete medium supplemented with the same concentration of GM-CSF or M-CSF. BMDC and BMDM were completely differentiated from bone marrow cells on day 7, separately.

IHC staining—Fresh skin tissue from mice were fixed immediately in 10% fresh neutral buffered formalin for 24 h. Samples were sectioned and stained with hematoxylin and eosin (H&E). Sections for IHC staining were deparaffinized and rehydrated before applying the primary antibody. For human FABP5 staining, samples were treated with Diva Decloaker (pH 9.0) at room temperature for 20 min and quenched of endogenous peroxidase activity using BLOXALL endogenous blocking solution (Cat. #SP-6000, Vector Laboratories). Samples were blocked with 2.5% normal horse serum (Cat. #MP-7405, Vector Laboratories) for 1 h at room temperature to prevent from non-specific staining. The anti-human FABP5 primary antibody (Cat. #AF1476, R&D Systems) were added into samples with dilution

of 1:25000, and incubated for 1 h at room temperature, then stained with biotinylated anti-goat secondary antibody with dilution of 1:500 and VECTASTAIN Elite ABC-HRP Kits (Cat#PK-6100, Vector Laboratories) for 30 min, separately. For neutrophil staining, samples were treated with 10 mM citrate buffer (pH 6.0) at room temperature for 20 min. After quenching of the endogenous peroxidase activity, samples were blocked and incubated with 1:800 anti-human neutrophil elastase antibody (Cat. #ab68672, Abcam) for 1 h at room temperature, then stained with Envision (HRP-rabbit) for 30 min. All methods were used with DAB (Cat. #K346811–2, Agilent) for 5 min and DAB Enhancer (Cat. #S196131–2, Agilent) for 3 min. Sections were subsequently counterstained with hematoxylin and mounted in the mounting medium. IHC images were taken with ECHO Revolve Microscope (RVL2-K) in bright-field mode using 4 ×, 10 ×, 20×, and 40× objective lenses, respectively.

Confocal analysis—Confocal microscopy was used for fluorescent imaging targeting multiple proteins in cells and tissues. For VCP and FABP5 localization analysis, HaCaT cells were seeded into the 35 mm glass bottom dish (Cat.#P35G-1.5–20-C, MatTek) for overnight culture. Cells were washed with 1 × PBS twice and fixed/permeabilized with cold methanol for 20 min. Samples were blocked with 5% BSA for 1 h at 4°C and ready to stain with goat anti-FABP5 antibody (Cat. #AF1476, R&D Systems), mouse anti-VCP antibody (Cat. #MA3–004, Fisher Scientific), and control antibodies (control rabbit IgG with Cat. #401501, Biolegend; control goat IgG with Cat. #AB-108-C, R&D Systems) at 4°C overnight, respectively. Samples were washed with 1 × PBS three times and added secondary antibodies were added (donkey anti-mouse IgG with Cat. #PA128626, Fisher Scientific; donkey anti-goat IgG with Cat. #705–546-147, Jackson Immuno Research) for 1 h staining at room temperature, respectively. Cell nuclei were stained with Hoechst33342 for 15 min at room temperature. All images were captured with a Zeiss Confocal Microscope, and images were analyzed by ImageJ software (NIH).

QUANTIFICATION AND STATISTICAL ANALYSIS

All data were presented as the mean ± SD unless notified specifically. All experiment as indicated were performed by at least three independent experiments or technical replicates. For both *in vitro* and *in vivo* experiments, a two-tailed, unpaired student t-test, two-way ANOVA followed by Bonferroni's multiple comparison test, were performed by GraphPad Prism 9. *$p < 0.05$, **$p < 0.01$, ***$p < 0.001$, ****$p < 0.0001$ are regarded as statistically significant.

Supplementary Material

Refer to Web version on PubMed Central for supplementary material.

ACKNOWLEDGMENTS

We thank the Comparative Pathology Laboratory at the University of Iowa for skin histological and immunohistochemistry staining and the Proteomic facility at the University of Iowa for mass spectrometry and comparative analysis with dimethyl-labeled samples. B.L. thanks the funding support from NIH grants R01AI137324, R01CA180986, and U01CA272424. Support for A.J. was provided by the Department of Veterans Affairs Biomedical Laboratory Research and Development Award I01BX004907 and NIH grant R01AR077194.

REFERENCES

1. Griffiths CE, and Barker JN (2007). Pathogenesis and clinical features of psoriasis. Lancet 370, 263–271. [PubMed: 17658397]
2. Gangwar RS, Gudjonsson JE, and Ward NL (2022). Mouse Models of Psoriasis: A Comprehensive Review. J. Invest. Dermatol. 142, 884–897. [PubMed: 34953514]
3. van der Fits L, Mourits S, Voerman JSA, Kant M, Boon L, Laman JD, Cornelissen F, Mus AM, Florencia E, Prens EP, and Lubberts E (2009). Imiquimod-induced psoriasis-like skin inflammation in mice is mediated via the IL-23/IL-17 axis. J. Immunol. 182, 5836–5845. [PubMed: 19380832]
4. Machado Á, and Torres T (2018). Guselkumab for the Treatment of Psoriasis. BioDrugs 32, 119–128. [PubMed: 29470778]
5. Singh S, Kroe-Barrett RR, Canada KA, Zhu X, Sepulveda E, Wu H, He Y, Raymond EL, Ahlberg J, Frego LE, et al. (2015). Selective targeting of the IL23 pathway: Generation and characterization of a novel high-affinity humanized anti-IL23A antibody. mAbs 7, 778–791. [PubMed: 25905918]
6. Deza G, Notario J, Lopez-Ferrer A, Vilarrasa E, Ferran M, Del Alcazar E, Carrascosa JM, Corral M, Salleras M, Ribera M, et al. (2019). Initial results of ixekizumab efficacy and safety in real-world plaque psoriasis patients: a multicentre retrospective study. J. Eur. Acad. Dermatol. Venereol. 33, 553–559. [PubMed: 30317679]
7. Papp KA, Merola JF, Gottlieb AB, Griffiths CEM, Cross N, Peterson L, Cioffi C, and Blauvelt A (2018). Dual neutralization of both interleukin 17A and interleukin 17F with bimekizumab in patients with psoriasis: Results from BE ABLE 1, a 12-week randomized, double-blinded, placebo-controlled phase 2b trial. J. Am. Acad. Dermatol. 79, 277–286.e10. [PubMed: 29609013]
8. Chiang CC, Cheng WJ, Korinek M, Lin CY, and Hwang TL (2019). Neutrophils in Psoriasis. Front. Immunol. 10, 2376. [PubMed: 31649677]
9. Rodriguez-Rosales YA, Langereis JD, Gorris MAJ, van den Reek JMPA, Fasse E, Netea MG, de Vries IJM, Gomez-Muñoz L, van Cranenbroek B, Körber A, et al. (2021). Immunomodulatory aged neutrophils are augmented in blood and skin of psoriasis patients. J. Allergy Clin. Immunol. 148, 1030–1040. [PubMed: 33745888]
10. Ikeda S, Takahashi H, Suga Y, Eto H, Etoh T, Okuma K, Takahashi K, Kanbara T, Seishima M, Morita A, et al. (2013). Therapeutic depletion of myeloid lineage leukocytes in patients with generalized pustular psoriasis indicates a major role for neutrophils in the immunopathogenesis of psoriasis. J. Am. Acad. Dermatol. 68, 609–617. [PubMed: 23332516]
11. Li B, Hao J, Zeng J, and Sauter ER (2020). SnapShot: FABP Functions. Cell 182, 1066–1066.e1. [PubMed: 32822569]
12. Hotamisligil GS (2006). Inflammation and metabolic disorders. Nature 444, 860–867. [PubMed: 17167474]
13. Senguttuvan NB, Ramakrishnan S, Singh S, and Mishra S (2015). Percutaneous management of coronary embolism with prosthetic heart valve thrombosis after Bentall's procedure. Indian Heart J. 67, 589–591. [PubMed: 26702693]
14. Ross R (1999). Atherosclerosis–an inflammatory disease. N. Engl. J. Med. 340, 115–126. [PubMed: 9887164]
15. Hao J, Zhang Y, Yan X, Yan F, Sun Y, Zeng J, Waigel S, Yin Y, Fraig MM, Egilmez NK, et al. (2018). Circulating Adipose Fatty Acid Binding Protein Is a New Link Underlying Obesity-Associated Breast/Mammary Tumor Development. Cell Metabol. 28, 689–705.e5.
16. Liao M, Liu Y, Yuan J, Wen Y, Xu G, Zhao J, Cheng L, Li J, Wang X, Wang F, et al. (2020). Single-cell landscape of bronchoalveolar immune cells in patients with COVID-19. Nat. Med. 26, 842–844. [PubMed: 32398875]
17. Siegenthaler G, Hotz R, Chatellard-Gruaz D, Jaconi S, and Saurat JH (1993). Characterization and expression of a novel human fatty acid-binding protein: the epidermal type (E-FABP). Biochem. Biophys. Res. Commun. 190, 482–487. [PubMed: 8427590]
18. Dallaglio K, Marconi A, Truzzi F, Lotti R, Palazzo E, Petrachi T, Saltari A, Coppini M, and Pincelli C (2013). E-FABP induces differentiation in normal human keratinocytes and modulates the differentiation process in psoriatic keratinocytes in vitro. Exp. Dermatol. 22, 255–261. [PubMed: 23528210]

19. Kannan-Thulasiraman P, Seachrist DD, Mahabeleshwar GH, Jain MK, and Noy N (2010). Fatty acid-binding protein 5 and PPARbeta/delta are critical mediators of epidermal growth factor receptor-induced carcinoma cell growth. J. Biol. Chem. 285, 19106–19115. [PubMed: 20424164]
20. Zhang Y, Li Q, Rao E, Sun Y, Grossmann ME, Morris RJ, Cleary MP, and Li B (2015). Epidermal Fatty Acid binding protein promotes skin inflammation induced by high-fat diet. Immunity 42, 953–964. [PubMed: 25992864]
21. Yin D, Hao J, Jin R, Yi Y, Bodduluri SR, Hua Y, Anand A, Deng Y, Haribabu B, Egilmez NK, et al. (2022). Epidermal Fatty Acid–Binding Protein Mediates Depilatory-Induced Acute Skin Inflammation. J. Invest. Dermatol. 142, 1824–1834.e7. [PubMed: 34942197]
22. Hao J, Jin R, Zeng J, Hua Y, Yorek MS, Liu L, Mandal A, Li J, Zheng H, Sun Y, et al. (2022). Consumption of fish oil high-fat diet induces murine hair loss via epidermal fatty acid binding protein in skin macrophages. Cell Rep. 41, 111804. [PubMed: 36516778]
23. Jin R, Hao J, Yi Y, Yin D, Hua Y, Li X, Bao H, Han X, Egilmez NK, Sauter ER, and Li B (2021). Dietary Fats High in Linoleic Acids Impair Antitumor T-cell Responses by Inducing E-FABP-Mediated Mitochondrial Dysfunction. Cancer Res. 81, 5296–5310. [PubMed: 34400394]
24. Zhang Y, Hao J, Zeng J, Li Q, Rao E, Sun Y, Liu L, Mandal A, Landers VD, Morris RJ, et al. (2018). Epidermal FABP Prevents Chemical-Induced Skin Tumorigenesis by Regulation of TPA-Induced IFN/p53/SOX2 Pathway in Keratinocytes. J. Invest. Dermatol. 138, 1925–1934. [PubMed: 29559340]
25. Armstrong AW, Harskamp CT, and Armstrong EJ (2013). Psoriasis and metabolic syndrome: a systematic review and meta-analysis of observational studies. J. Am. Acad. Dermatol. 68, 654–662. [PubMed: 23360868]
26. Nowowiejska J, Baran A, and Flisiak I (2021). Aberrations in Lipid Expression and Metabolism in Psoriasis. Int. J. Mol. Sci. 22, 6561. [PubMed: 34207318]
27. Ogawa E, Owada Y, Ikawa S, Adachi Y, Egawa T, Nemoto K, Suzuki K, Hishinuma T, Kawashima H, Kondo H, et al. (2011). Epidermal FABP (FABP5) regulates keratinocyte differentiation by 13(S)-HODE-mediated activation of the NF-kappaB signaling pathway. J. Invest. Dermatol. 131, 604–612. [PubMed: 21068754]
28. Zhang X, Kluger Y, Nakayama Y, Poddar R, Whitney C, DeTora A, Weissman SM, and Newburger PE (2004). Gene expression in mature neutrophils: early responses to inflammatory stimuli. J. Leukoc. Biol. 75, 358–372. [PubMed: 14634056]
29. Tortola L, Rosenwald E, Abel B, Blumberg H, Schäfer M, Coyle AJ, Renauld JC, Werner S, Kisielow J, and Kopf M (2012). Psoriasiform dermatitis is driven by IL-36-mediated DC-keratinocyte crosstalk. J. Clin. Invest. 122, 3965–3976. [PubMed: 23064362]
30. Anderton H, Chopin M, Dawson CA, Nutt SL, Whitehead L, Silke N, Lalaloui N, and Silke J (2022). Langerhans cells are an essential cellular intermediary in chronic dermatitis. Cell Rep. 39, 110922. [PubMed: 35675765]
31. Zhang X, Li X, Wang Y, Chen Y, Hu Y, Guo C, Yu Z, Xu P, Ding Y, Mi QS, et al. (2022). Abnormal lipid metabolism in epidermal Langerhans cells mediates psoriasis-like dermatitis. JCI Insight 7, e150223. [PubMed: 35801590]
32. Liu T, Zhang L, Joo D, and Sun SC (2017). NF-kappaB signaling in inflammation. Signal Transduct. Target. Ther. 2, 17023. [PubMed: 29158945]
33. Tourniaire F, Romier-Crouzet B, Lee JH, Marcotorchino J, Gouranton E, Salles J, Malezet C, Astier J, Darmon P, Blouin E, et al. (2013). Chemokine Expression in Inflamed Adipose Tissue Is Mainly Mediated by NF-kappaB. PLoS One 8, e66515. [PubMed: 23824685]
34. Zhang Z, Wang Y, Li C, Shi Z, Hao Q, Wang W, Song X, Zhao Y, Jiao S, and Zhou Z (2015). The Transitional Endoplasmic Reticulum ATPase p97 Regulates the Alternative Nuclear Factor NF-kappaB Signaling via Partial Degradation of the NF-kappaB Subunit p100. J. Biol. Chem. 290, 19558–19568. [PubMed: 26112410]
35. Li JM, Wu H, Zhang W, Blackburn MR, and Jin J (2014). The p97-UFD1L-NPL4 protein complex mediates cytokine-induced IkappaBalpha proteolysis. Mol. Cell Biol. 34, 335–347. [PubMed: 24248593]
36. Penna RP (1990). Manpower trends and the role of educators in preparing students for postgraduate training. Am. J. Hosp. Pharm. 47, 92–98. [PubMed: 2301433]

37. Cardili RN, Deghaide NS, Mendes-Junior CT, Donadi EA, and Souza CS (2016). HLA-C and TNF gene polymorphisms are associated with psoriasis in Brazilian patients. Int. J. Dermatol. 55, e16–e22. [PubMed: 26470763]
38. Nestle FO, Kaplan DH, and Barker J (2009). Psoriasis. N. Engl. J. Med. 361, 496–509. [PubMed: 19641206]
39. Boehncke WH, and Schön MP (2015). Psoriasis. Lancet 386, 983–994. [PubMed: 26025581]
40. Gao Y, Yao X, Zhai Y, Li L, Li H, Sun X, Yu P, Xue T, Li Y, and Hu Y (2021). Single cell transcriptional zonation of human psoriasis skin identifies an alternative immunoregulatory axis conducted by skin resident cells. Cell Death Dis. 12, 450. [PubMed: 33958582]
41. Mrowietz U (2017). Neutrophils' sexiness is independent of trendy fashion. Exp. Dermatol. 26, 312–313. [PubMed: 27248359]
42. Jaillon S, Galdiero MR, Del Prete D, Cassatella MA, Garlanda C, and Mantovani A (2013). Neutrophils in innate and adaptive immunity. Semin. Immunopathol. 35, 377–394. [PubMed: 23553214]
43. Nauseef WM, and Borregaard N (2014). Neutrophils at work. Nat. Immunol. 15, 602–611. [PubMed: 24940954]
44. Schön MP, Broekaert SMC, and Erpenbeck L (2017). Sexy again: the renaissance of neutrophils in psoriasis. Exp. Dermatol. 26, 305–311. [PubMed: 27194625]
45. Yuan ZC, Xu WD, Liu XY, Liu XY, Huang AF, and Su LC (2019). Biology of IL-36 Signaling and Its Role in Systemic Inflammatory Diseases. Front. Immunol. 10, 2532. [PubMed: 31736959]
46. Koss CK, Wohnhaas CT, Baker JR, Tilp C, Przibilla M, Lerner C, Frey S, Keck M, Williams CMM, Peter D, et al. (2021). IL36 is a critical upstream amplifier of neutrophilic lung inflammation in mice. Commun. Biol. 4, 172. [PubMed: 33558616]
47. Armstrong EH, Goswami D, Griffin PR, Noy N, and Ortlund EA (2014). Structural basis for ligand regulation of the fatty acid-binding protein 5, peroxisome proliferator-activated receptor beta/delta (FABP5-PPARbeta/delta) signaling pathway. J. Biol. Chem. 289, 14941–14954. [PubMed: 24692551]
48. Morgan E, Kannan-Thulasiraman P, and Noy N (2010). Involvement of Fatty Acid Binding Protein 5 and PPARbeta/delta in Prostate Cancer Cell Growth. PPAR Res. 2010, 234629. [PubMed: 20847935]
49. Dai RM, Chen E, Longo DL, Gorbea CM, and Li CC (1998). Involvement of valosin-containing protein, an ATPase Co-purified with IkappaBalpha and 26 S proteasome, in ubiquitin-proteasome-mediated degradation of IkappaBalpha. J. Biol. Chem. 273, 3562–3573. [PubMed: 9452483]
50. Schweitzer K, Pralow A, and Naumann M (2016). p97/VCP promotes Cullin-RING-ubiquitin-ligase/proteasome-dependent degradation of IkappaBalpha and the preceding liberation of RelA from ubiquitinated IkappaBalpha. J. Cell Mol. Med. 20, 58–70. [PubMed: 26463447]
51. Goldminz AM, Au SC, Kim N, Gottlieb AB, and Lizzul PF (2013). NF-kappaB: an essential transcription factor in psoriasis. J. Dermatol. Sci. 69, 89–94. [PubMed: 23219896]
52. El Dein Mohamed AS, Hagag MM, Kassem NMAEA, and Shehata WA (2021). Valosin-containing Protein in Psoriasis: A Clinical and Immunohistochemical Study. Appl. Immunohistochem. Mol. Morphol. 29, e68–e72. [PubMed: 33979096]
53. Larangé A, Antonios D, Pallardy M, and Kerdine-Römer S (2009). TLR7 and TLR8 agonists trigger different signaling pathways for human dendritic cell maturation. J. Leukoc. Biol. 85, 673–683. [PubMed: 19164127]
54. Hemmi H, Kaisho T, Takeuchi O, Sato S, Sanjo H, Hoshino K, Horiuchi T, Tomizawa H, Takeda K, and Akira S (2002). Small anti-viral compounds activate immune cells via the TLR7 MyD88-dependent signaling pathway. Nat. Immunol. 3, 196–200. [PubMed: 11812998]
55. Yao Y, Richman L, Morehouse C, de los Reyes M, Higgs BW, Boutrin A, White B, Coyle A, Krueger J, Kiener PA, and Jallal B (2008). Type I interferon: potential therapeutic target for psoriasis? PLoS One 3, e2737. [PubMed: 18648529]
56. Nair RP, Duffin KC, Helms C, Ding J, Stuart PE, Goldgar D, Gudjonsson JE, Li Y, Tejasvi T, Feng BJ, et al. (2009). Genome-wide scan reveals association of psoriasis with IL-23 and NF-kappaB pathways. Nat. Genet. 41, 199–204. [PubMed: 19169254]

57. Han H, Cho JW, Lee S, Yun A, Kim H, Bae D, Yang S, Kim CY, Lee M, Kim E, et al. (2018). TRRUST v2: an expanded reference database of human and mouse transcriptional regulatory interactions. Nucleic Acids Res. 46, D380–D386. [PubMed: 29087512]

58. Donato M, Xu Z, Tomoiaga A, Granneman JG, Mackenzie RG, Bao R, Than NG, Westfall PH, Romero R, and Draghici S (2013). Analysis and correction of crosstalk effects in pathway analysis. Genome Res. 23, 1885–1893. [PubMed: 23934932]

59. Draghici S, Khatri P, Tarca AL, Amin K, Done A, Voichita C, Georgescu C, and Romero R (2007). A systems biology approach for pathway level analysis. Genome Res. 17, 1537–1545. [PubMed: 17785539]

60. Yu CL, Summers RM, Li Y, Mohanty SK, Subramanian M, and Pope RM (2015). Rapid identification and quantitative validation of a caffeine-degrading pathway in Pseudomonas sp. J. Proteome Res. 14, 95–106. [PubMed: 25350919]

61. Boukamp P, Petrussevska RT, Breitkreutz D, Hornung J, Markham A, and Fusenig NE (1988). Normal keratinization in a spontaneously immortalized aneuploid human keratinocyte cell line. J. Cell Biol. 106, 761–771. [PubMed: 2450098]

Highlights

- Psoriasis is associated with increased levels of FABP5 in the inflammatory skin tissue
- FABP5 deficiency in mice, particularly in keratinocytes, alleviates psoriatic inflammation
- FABP5 specifically promotes neutrophil infiltration during the initiation of psoriasis
- FABP5/VCP axis mediates NF-κB/neutrophil chemotaxis and activation in keratinocytes

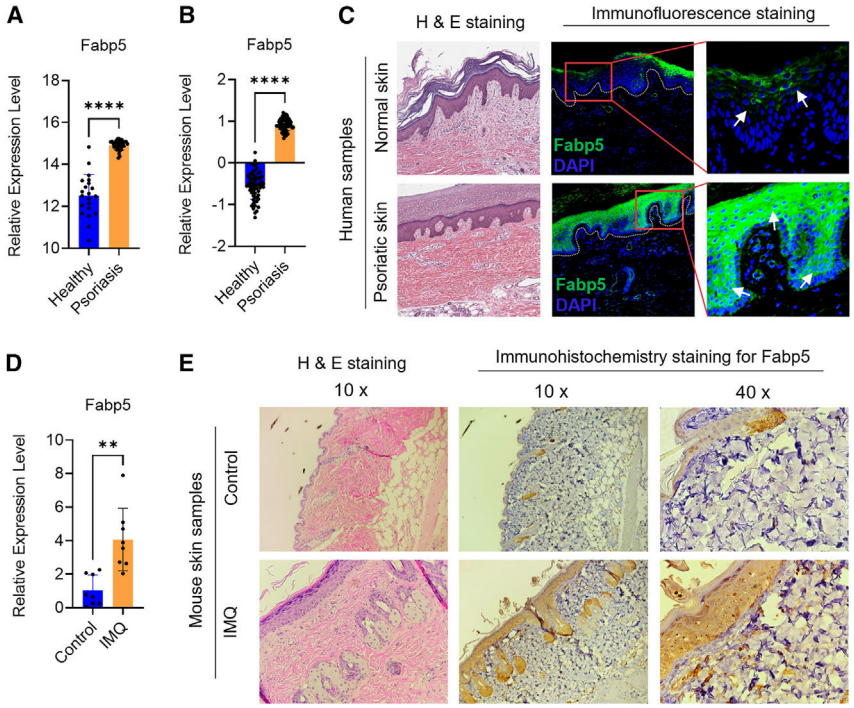

Figure 1. The increasing levels of FABP5 are associated with psoriasis.

(A) FABP5 levels in skin samples from healthy individuals and patients with psoriasis. Data were analyzed by publicly accessing database GSE14905 from the Gene Expression Omnibus (GEO). The database of GSE14905 contained 21 healthy individuals and 33 psoriasis patients.

(B) FABP5 levels in skin samples from healthy individuals and patients with psoriasis. Data were analyzed by publicly accessing GEO database GSE13355, which contained 64 healthy individuals and 58 psoriasis patients.

(C) Alexa Fluor 488-labeled FABP5 expression profile in human skin tissue collected from psoriasis patients (lower panels) and healthy individuals (upper panels). H&E staining (left panels) showed the structure of skin tissue from psoriasis patients and healthy individuals.

(D) Fabp5 mRNA levels in skin tissues from imiquimod (IMQ)-induced psoriasis mice and normal mice (n = 8/group).

(E) H&E staining (left panels) and immunohistochemistry staining (right panels) showed the structure of skin tissue and Fabp5 levels from IMQ-induced psoriasis mice and control mice, respectively. Data are shown as mean ± SD in (A, B, and D) (**$p \leq 0.01$, ****$p \leq 0.0001$ as compared with healthy or control groups, unpaired Student's t test). See also Figure S1.

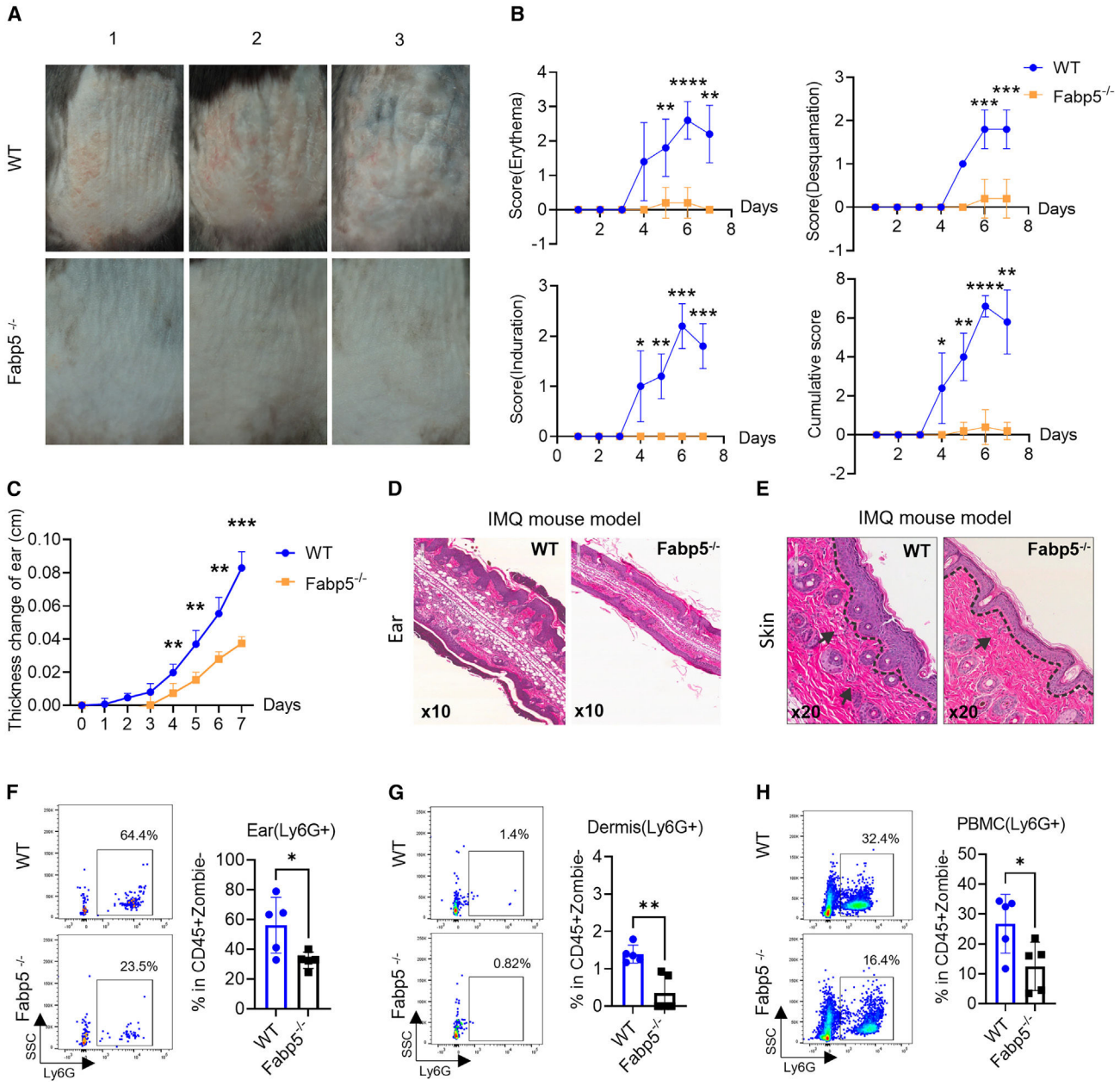

Figure 2. Fabp5 deficiency attenuated IMQ-induced psoriasis progression with less neutrophil infiltration.

(A) Representative images of skin from Fabp5 global knockout and WT mice after treatment with IMQ for 7 days. On day 7 and WT controls.

(B) The score of erythema, induration, and desquamation on skin were evaluated from the first day on both Fabp5 global knockout mice and WT controls. The cumulative score was calculated in a sum of the score of erythema, induration, and desquamation at the indicated time point (n = 5/group).

(C) Ear thickness was measured daily for both strains, and its change was calculated by subtracting the first day value (n = 5/group).

(D and E) H&E staining for ear (D) and skin (E) from both Fabp5 global knockout mice and WT controls.

(F–H) Neutrophil infiltration and ratio were analyzed from ear (F), dermis (G), and PBMC (H) using flow cytometry at the endpoint of treatment for both Fabp5 global knockout mice and WT controls. In each figure, left panel: representative flow plot with gate on neutrophils ($Ly6G^+$) from Fabp5 global knockout mice and WT controls. The parent population is $CD45^+Zombie^-$; right panel: histogram represents neutrophil ratio in different skin tissues (n = 5/group). Data are shown as mean ± SD in (B, C, and F–H) (*p ≤ 0.05, **p ≤ 0.01, ***p ≤ 0.001, ****p ≤ 0.0001 as compared with healthy or control groups, unpaired Student's t test). See also Figure S2.

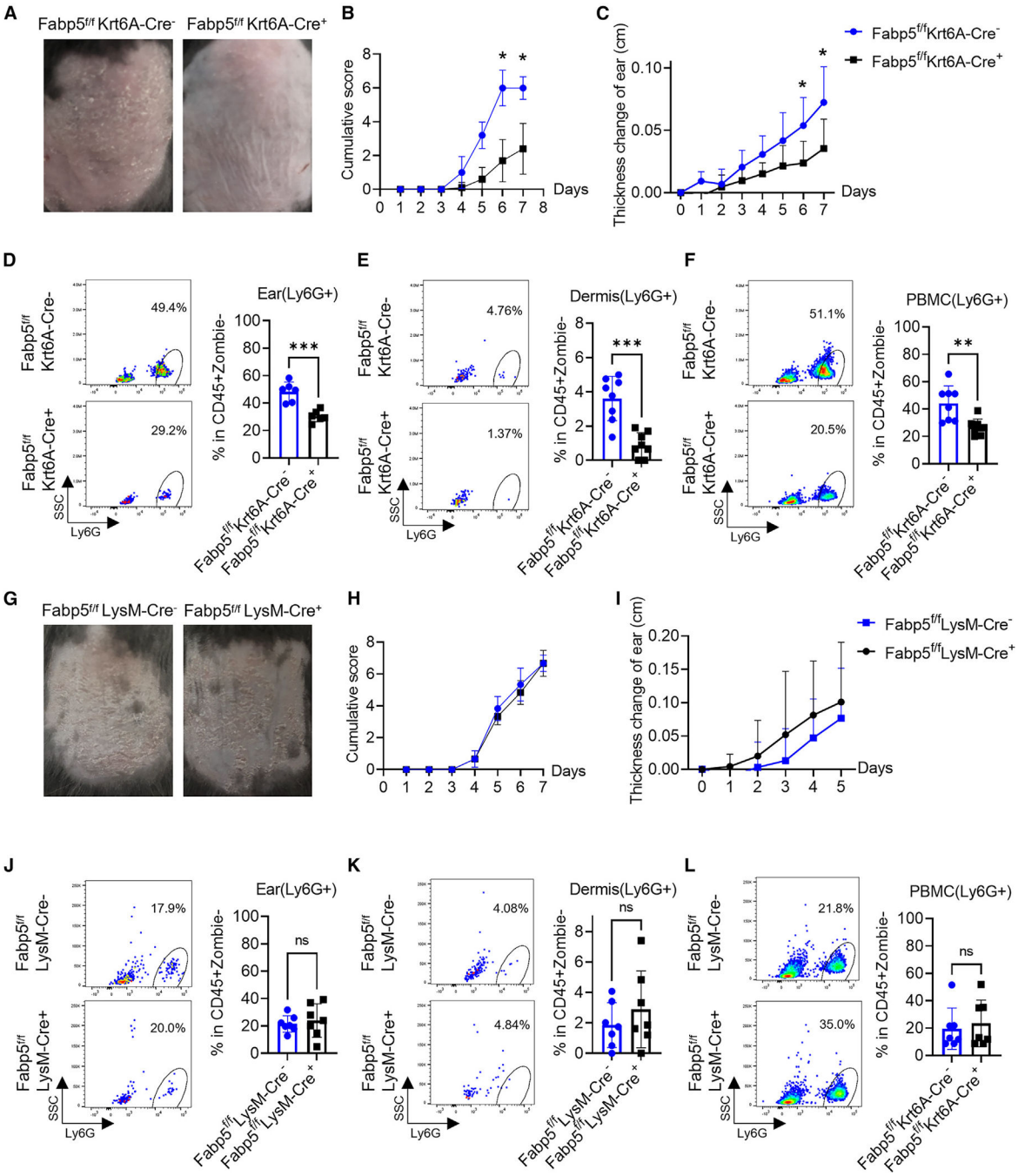

Figure 3. Fabp5 deficiency in keratinocyte but not in myeloid cells attenuated neutrophil infiltration.

(A) Representative images of the skin from Fabp5$^{f/f}$ Krt6A-Cre^{+} and Fabp5$^{f/f}$ Krt6A-Cre^{-} mice after treatment with IMQ for 7 days.

(B) The cumulative score (a sum score of erythema, induration, and desquamation on skin) was calculated from the first day on both Fabp5$^{f/f}$ Krt6A-Cre^{+} and Fabp5$^{f/f}$ Krt6A-Cre^{-} mice (n = 10/group).

(C) Ear thickness was measured daily from Fabp5$^{f/f}$ Krt6A-Cre^{+} and Fabp5$^{f/f}$ Krt6A-Cre^{-}, and its change was calculated by subtracting the first day value (n = 10/group).

(D) Neutrophil infiltration and its ratio were analyzed from the ear using flow cytometry at the endpoint of treatment for both Fabp5$^{f/f}$ Krt6A-Cre^{+} and Fabp5$^{f/f}$ Krt6A-Cre^{-} mice. In each figure, left panel: representative flow plot with gate on neutrophils (Ly6G^{+}) from Fabp5 global knockout mice and WT controls. The parent population is CD45^{+}Zombie^{-}; right panel: histogram represents neutrophil ratio in different tissues (n = 6/group).
(E and F) Neutrophils infiltration and ratio were analyzed from the ear (D), dermis (E), and PBMC (F) using flow cytometry at the endpoint of treatment for both Fabp5$^{f/f}$ Krt6A-Cre^{+} and Fabp5$^{f/f}$ Krt6A-Cre^{-} mice. In each figure, left is the flow plot with gate on neutrophils (Ly6G^{+}) in Fabp5 global knockout and WT mice. The parent population is CD45^{+}Zombie^{-}; right is the histogram showing neutrophil ratio in individual tissues (n = 8/group).
(G) Images were taken from skin with IMQ-induced psoriasis on day 7 from Fabp5$^{f/f}$ LysM-Cre^{+} and Fabp5$^{f/f}$ LysM-Cre^{-}.
(H) Ear thickness was measured daily from Fabp5$^{f/f}$ LysM-Cre^{+} and Fabp5$^{f/f}$ LysM-Cre^{-}, and its change was calculated by subtracting the first day value (n = 6/group).
(I) The cumulative score (a sum score of erythema, induration, and desquamation on skin) was calculated from the first day on both Fabp5$^{f/f}$ LysM-Cre^{+} and Fabp5$^{f/f}$ LysM-Cre^{-} mice (n = 6/group).
(J–L) Neutrophils infiltration and its ratio was analyzed from the ear (J), dermis (K), and PBMC (L) using flow cytometry at the endpoint of treatment for both Fabp5$^{f/f}$ LysM-Cre^{+} and Fabp5$^{f/f}$ LysM-Cre^{-} mice. In each panel, flow cytometric plot (left) showed neutrophils (Ly6G^{+}) population in Fabp5 global knockout and WT mice; histogram (right) represented neutrophil ratio in CD45^{+} immune cells in individual tissues (n = 7/group). Data are shown as mean ± SD in (D–F, K, and L) (*$p \leq 0.05$, **$p \leq 0.01$, ***$p \leq 0.001$; ns, not significant compared with control groups, unpaired Student’s t test). See also Figures S3 and S4.

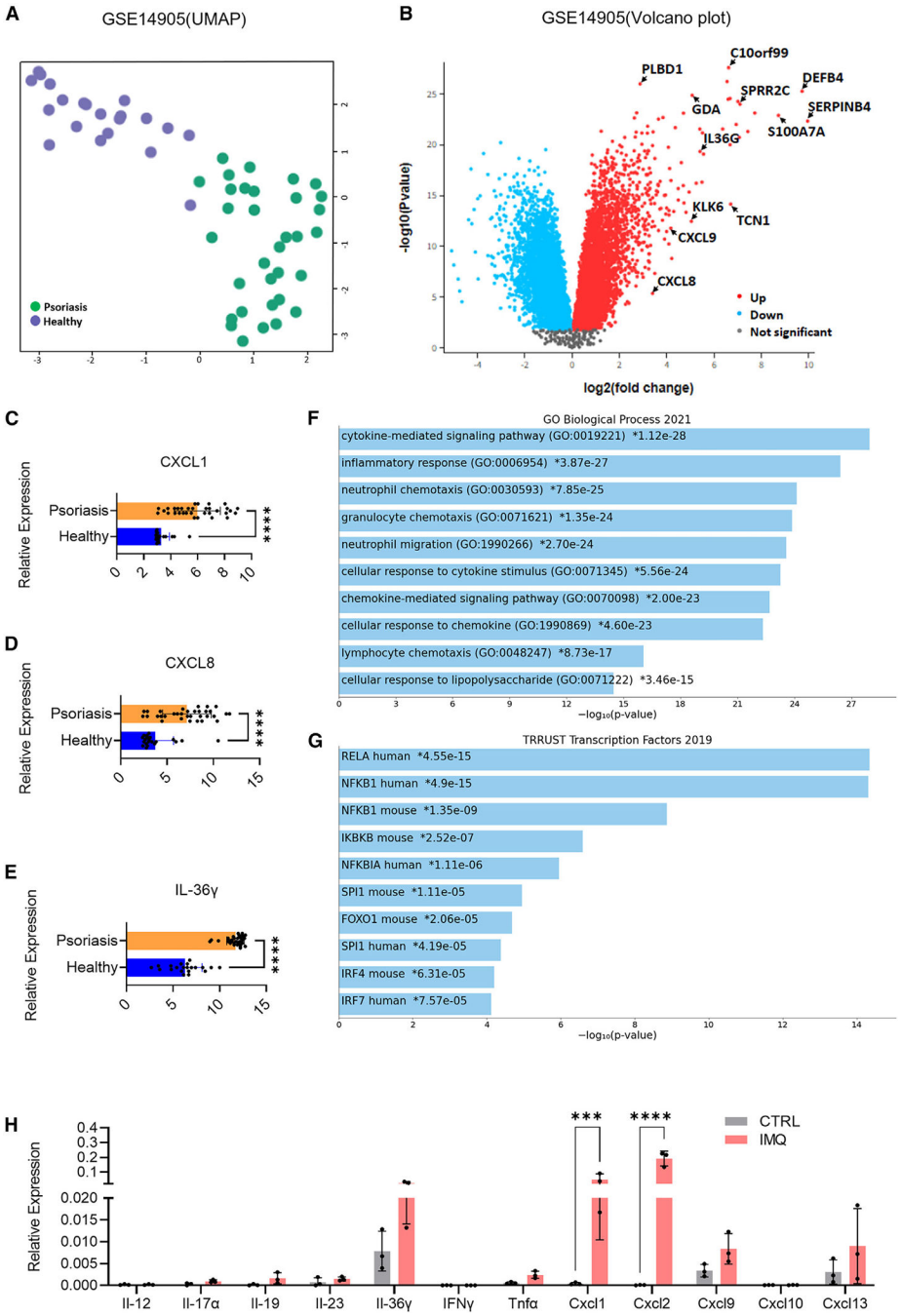

Figure 4. Human psoriasis is associated with NFκB-mediated chemokine signaling.

(A) The Uniform Manifold Approximation and Projection showed two different clusters, which are healthy samples (green, n = 21) and psoriasis samples (blue, n = 33).

(B) The differentially expressed genes (DEGs) from volcano plot with an adjusted p value cutoff of 0.05 (red dots are upregulated genes, blue dots are downregulated genes, gray dots are genes with no significance).

(C–E) Relative expression of CXCL1 (C), CXCL8 (D), and IL-36 γ (E) in skin samples from healthy individuals and lesional skin samples from patients with psoriasis. Data were

analyzed by publicly accessing the GSE14905 database. This database contains 21 healthy individuals and 33 psoriasis patients.

(F) The analysis of gene ontology biological process (version 2021) from top hits cytokines indicated the most important signaling pathways.

(G) The most relevant transcription factors were predicted by the analysis of transcriptional regulatory relationships unraveled by sentence-based text mining (TRRUST).

(H) Real-time PCR for cytokine expression in skin tissue on both IMQ-treated mice and control mice. Data were analyzed by two-way ANOVA followed by Bonferroni's multiple comparison test (n = 3/group). Data are shown as mean ± SD in (C–E and H) (****$p < 0.0001$ compared with control groups, unpaired Student's t test). See also Figure S5.

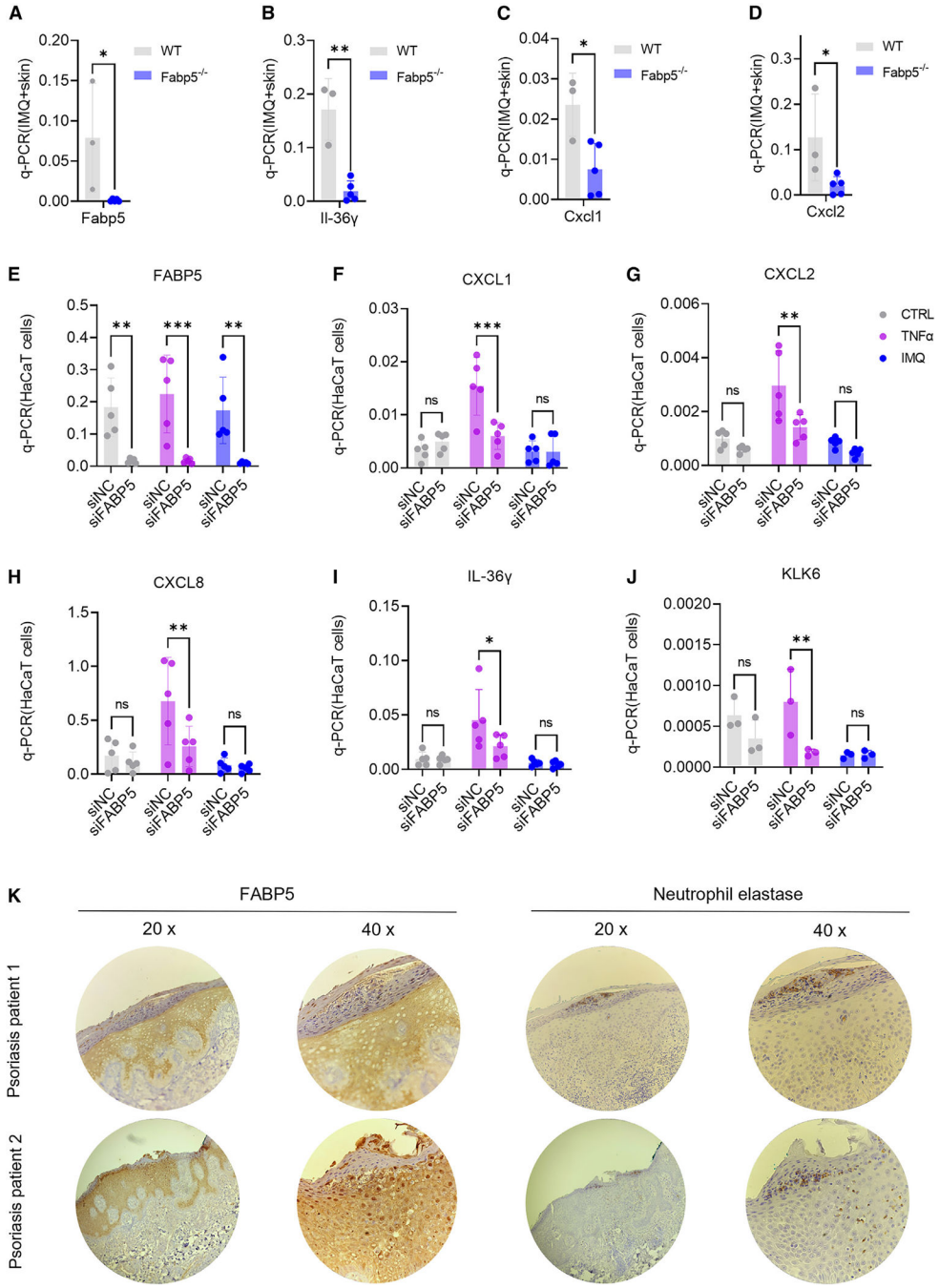

Figure 5. Silencing FABP5 in HaCaT cells inhibits TNF-α-induced neutrophil chemotaxis.

(A–D) Real-time PCR showed downregulation of Fabp5 (A), IL-36γ (B), Cxcl1 (C), and Cxcl2 (D) with IMQ-treated skin tissue for 24 h in Fabp5 global knockout mice compared with WT controls (n = 3/group).

(E–J) Real-time PCR showed the levels of FABP5 (E), CXCL1 (F), CXCL2 (G), CXCL8 (H), IL-36γ (I), and KLK6 (J) were downregulated in FABP5-deficient HaCaT cells transfected with 40 nM siRNA compared with siNC controls with 10 ng/mL TNF-α, 50 μg/mL IMQ, and DMSO as control treatment for 6 h (n = 5/group).

(K) Immunohistochemistry staining on skin tissues from two representative psoriasis patients showed FABP5 expression (left) and neutrophil elastase expression (right). Data are shown as mean ± SD in (A–J) (*$p \leq 0.05$, **$p \leq 0.01$, ***$p \leq 0.001$; ns, not significant compared with control groups, unpaired Student's t test). See also Figure S6.

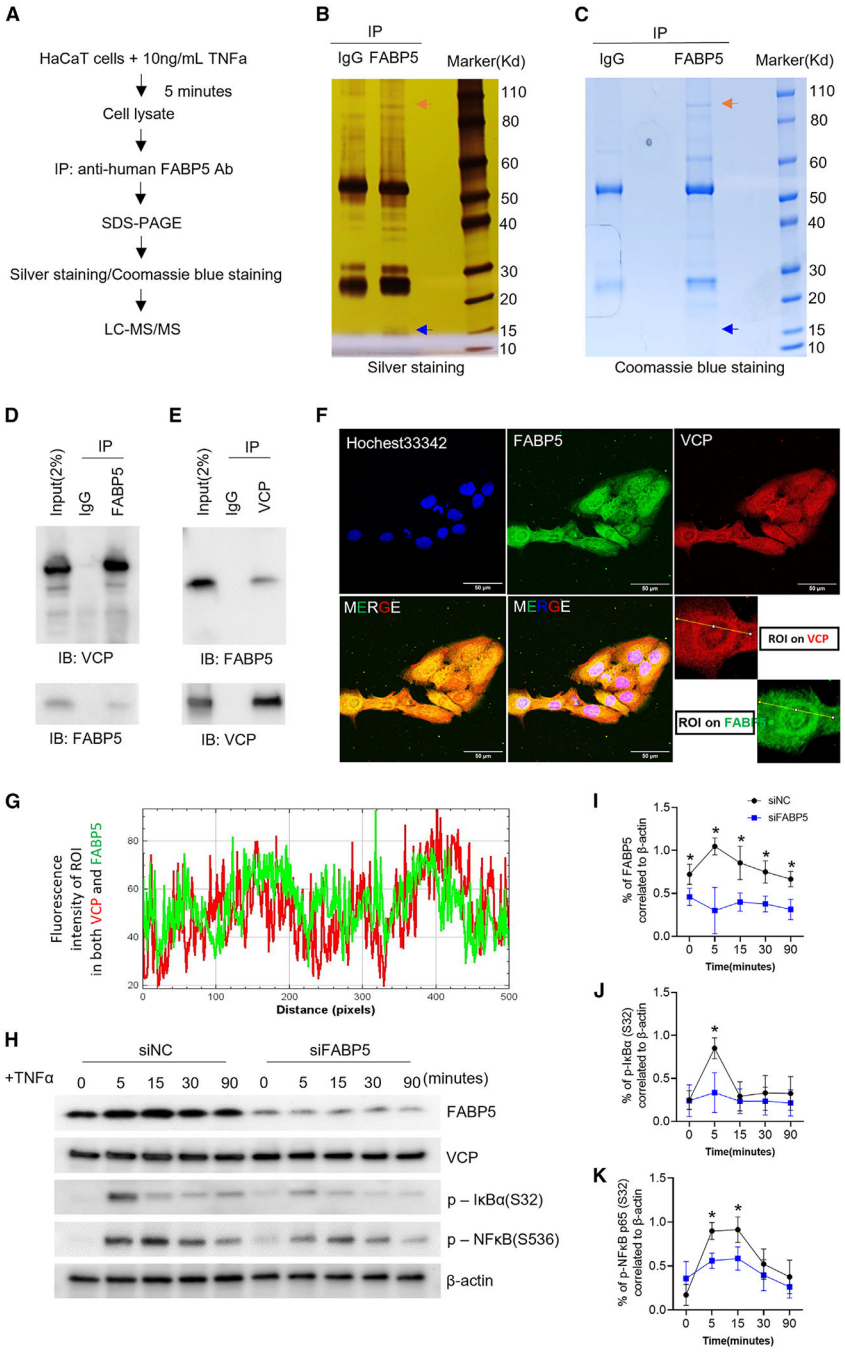

Figure 6. FABP5-VCP interaction promotes the TNF-α-induced NF-κB signaling pathway.

(A) The workflow on immunoprecipitation with anti-FABP5 antibody in HaCaT cells.

(B and C) Silver staining (B) and Coomassie blue staining (C) on SDS-PAGE gel for immunoprecipitated complexes. Blue arrow shows the band for FABP5, and orange arrow shows the band for VCP.

(D and E) Validation of FABP5-VCP interaction using immunoprecipitation and western blot. HaCaT lysates were immunoprecipitated (IP) with anti-FABP5 antibody (D) and anti-

VCP antibody (E), separately. Immunoblots were performed with anti-VCP antibody and anti-FABP5 antibody as indicated in the figure.

(F and G) Images of HaCaT cells show co-localization of FABP5 and VCP using confocal analysis (F). The straight line indicates the region of interest (ROI) utilized to measure the fluorescence intensity in both VCP and FABP5 (G). FABP5 (green), VCP (red), Hochest33342 (blue). Scale bars, 50 μm.

(H) Detection of NF-κB signaling activation using western blot. Transient silencing FABP5 with RNAi for 24 h in HaCaT cells and controls were treated with 10 ng/mL TNF-α for the indicated time points. FABP5, VCP, p-IκBα(S32), and p-NFκB(S536) were detected. β-Actin was used as internal control.

(I–K) The levels of p-IκBα(S32), p-NFκB p65 (S536), and FABP5 were quantified using ImageJ from three independent western blots experiments (*$p < 0.05$). Data are shown as mean ± SD in (I–K) (*$p \leq 0.05$ compared with the siNC control group, unpaired Student's t test). See also Figure S7.

KEY RESOURCES TABLE

REAGENT or RESOURCE	SOURCE	IDENTIFIER
Antibodies		
Rat monoclonal anti-mouse CD4-BV510	Biolegend	Cat#100449; RRID:AB_2564587
Rat monoclonal anti-mouse CD4-APC	Biolegend	Cat#100412; RRID:AB_312697
Rat monoclonal anti-mouse CD8α-BV605	Biolegend	Cat#100743; RRID:AB_2561352
Rat monoclonal anti-mouse CD8α-BV650	Biolegend	Cat#100742; RRID:AB_312747
Rat monoclonal anti-mouse/human CD11b-PE	Biolegend	Cat#101208; RRID:AB_312791
Rat monoclonal anti-mouse CD16/32	Biolegend	Cat#101302; RRID:AB_312801
Rat monoclonal anti-mouse CD45-Alexa Fluor 488	Biolegend	Cat#103122; RRID:AB_2562559
Rat monoclonal anti-mouse F4/80-PE	Biolegend	Cat#123110; RRID:AB_893486
Rat monoclonal anti-mouse F4/80-PE/Dazzle594	Biolegend	Cat#123146; RRID:AB_2564133
Rat monoclonal anti-mouse Ly6G-PE	Biolegend	Cat#127608; RRID:AB_1186099
Mouse monoclonal anti-mouse/human CD207(Langerin)-PE	Biolegend	Cat#144204; RRID:AB_2561499
Rat monoclonal anti-mouse TNFα-APC-Cy7	Biolegend	Cat#506344; RRID:AB_2565953
Hamster monoclonal anti-mouse TCRγδ-BV510	Biolegend	Cat#118131; RRID:AB_2563534
Hamster monoclonal anti-mouse CD3- APC-Cy7	BD Biosciences	Cat#561042, RRID:AB_2034003
Rat monoclonal anti-mouse CD11b- BUV737	BD Biosciences	Cat#612800; RRID:AB_2871093
Rabbit polyclonal anti-human/mouse Neutrophil elastase	Abcam	Cat#ab68672, RRID:AB_1658868
Rabbit polyclonal anti-mouse cytokeratin 6A	Proteintech	Cat#10590-1-AP, RRID:AB_2134306
Rabbit IgG control	Abcam	Cat#ab37415, RRID:AB_2631996
Rabbit polyclonal anti-human FABP5	Invitrogen	Cat#PA5-80612, RRID:AB_2787908
Mouse monoclonal anti-human VCP	Invitrogen	Cat#MA3-004, RRID:AB_2214638
Goat polyclonal anti-human/mouse FABP5	R&D Systems	Cat#AF1476; RRID:AB_2293656
Goat polyclonal normal IgG control	R&D Systems	Cat#AB-108-C; RRID:AB_354267
Rabbit polyclonal anti-human FABP5	R&D Systems	N/A
Mouse monoclonal IgG2a isotype control	Cell signaling technology	Cat#61656; RRID:AB_2799613
Rabbit monoclonal anti-human/mouse Phosphorylated IκBα(S32)	Cell signaling technology	Cat#2859S; RRID:AB_561111
Rabbit monoclonal anti-human/mouse Phosphorylated NF-κB(S536)	Cell signaling technology	Cat#3033S; RRID:AB_331284
Mouse monoclonal anti-human β-actin	Biolegend	Cat#643802; RRID:AB_2223199
Chemicals, peptides, and recombinant proteins		
Zombie Violet™ Fixable Viability Kit	Biolegend	Cat#423108
Cell Activation Cocktail	Biolegend	Cat#423303
eBioscience™ Foxp3/Transcription Factor Staining Buffer Set	Invitrogen	Cat#00-5523-00
0.25% Trpsin-EDTA (1X)	Gibco	Cat#25200056
Collagenase type 2	Worthington Biochemical	Cat#LS004177
Hyaluronidase	MP Biomedicals	Cat#0215127590
DNase I	ZYMO research	Cat#E1009-A
Hochest33342	Thermo Scientific	Cat#62249

REAGENT or RESOURCE	SOURCE	IDENTIFIER
Recombinant Human TNFα	Biolegend	Cat#570104
Recombinant Mouse TNFα	Biolegend	Cat#575204
Recombinant Mouse GM-CSF	Biolegend	Cat#576304
Recombinant Mouse M-CSF	Biolegend	Cat#576404
Imiquimod Cream, 5%	Perrigo	Cat#45802-368-62
Imiquimod	Sigma-Aldrich	Cat#I5159-200MG
Nair hair remover lotion	Nair	Product#00022600223290
Critical commercial assays		
PureLink RNA mini kit	Invitrogen	Cat#12183025
QuantiTect reverse transcription kit	Qiagen	Cat#205314
ImmPRESS® HRP Horse Anti-Rabbit IgG Polymer Detection Kit, Peroxidase	Vector	Cat#MP-7401-50
BLOXALL® Endogenous Blocking Solution, Peroxidase and Alkaline Phosphatase	Vector	SP-6000-100
Real-time PCR Primers	Table S1	N/A
DsiRNA for human FABP5	IDT	Cat#HSC.RNAI.N001444.12.1
DsiRNA for human VCP	IDT	Cat#HS.RI.VCP13.1
Power SYBR Green PCR Master Mix	Applied Biosystems	Cat#4368708
Deposited data		
Microarray data (PLOS ONE)	PMID:18648529	https://www.ncbi.nlm.nih.gov/geo/query/acc.cgi?acc=GSE14905
Microarray data (Nature Genetics)	PMID:19169254	https://www.ncbi.nlm.nih.gov/geo/query/acc.cgi?acc=GSE13355
Experimental models: Cell lines		
HaCaT cells	Donation	Dr. Klingelhutz Lab
BMDM	This paper	N/A
BMDC	This paper	N/A
Experimental models: Organisms/strains		
Mouse: Fabp5 KO/C57BL6J	This paper	N/A
Mouse: Fabp5 WT/C57BL6J	This paper	N/A
Mouse: Fabp5 f/f LysM-Cre−/C57BL6J	This paper	N/A
Mouse: Fabp5 f/f LysM-Cre+/C57BL6J	This paper	N/A
Mouse: Fabp5 f/f LysM-Cre−/C57BL6J	This paper	N/A
Mouse: Fabp5 f/f Krt6A-Cre−/C57BL6J	This paper	N/A
Mouse: Fabp5 f/f Krt6A-Cre+/C57BL6J	This paper	N/A
Oligonucleotides		
Real-time PCR Primers	Table S1	N/A
Software and algorithms		

REAGENT or RESOURCE	SOURCE	IDENTIFIER
FlowJo v10	BD Biosciences	www.flowjo.com
GraphPad Prism 8	GraphPad Software	www.graphpad.com
ImageJ	NIH	N/A
CoreIDRAW X7	CoreIDRAW	www.coreldraw.com